Memoirs of the School of Engineering, Nagoya University
Vol.44, No.1 (1992)

SIMULATION METHODS FOR FLUIDITY OF FRESH CONCRETE

Hiroshi MORI and Yasuo TANIGAWA

Department of Architecture

(Received May 29, 1992)

Abstract

In the present paper, three types of analytical methods for simulating the flowing behavior of fresh concrete, i.e., viscoplastic finite element method (VFEM), viscoplastic suspension element method (VSEM) and viscoplastic divided space element method (VDEM), are proposed, and some analytical results are shown. The deformation of fresh concrete in various consistency and rheological tests, such as slump test, flow test, VB test, vibrating slump test, vibrating consistency test and cylindrical rotation viscometer, and under various conditions of concreting works, such as casting, consolidating and pumping in pipe, is obtained by these simulation methods. The adequacy of the analytical methods is examined by comparison with experimental results, and the relationship between workability and rheological constants of fresh concrete is discussed.

1. Introduction

There are a number of experimental studies[1] on the measurement of the viscosity of concrete, mortar and cement paste in the fresh state. However, a definite method for predicting the flow and deformation of fresh concrete has not yet been proposed.

It is important to predict the behavior of fresh concrete at various stages, such as mixing, transporting, placing, consolidating, etc. Recently, a number of fundamental investigations on fresh concrete have been reported from the point of view of rheology[2,3], in which fresh concrete is considered as a kind of highly concentrated suspension and in which the analysis of its deformation is considered more or less possible by using rheological constants.

The slump test and the flow test are the most general methods used to judge the consistency of fresh concrete or mortar, and it is necessary to establish the relationship between the values obtained by these tests and the rheological constants such as plastic viscosity and yield value for a Bingham model[3]. Such investigations have been carried out based on experiments[4] or simple calculations[5].

The purpose of the present paper is to investigate simulation methods for the flowing behavior of fresh concrete. Three types of analytical methods, i.e., viscoplastic finite element method (VFEM), viscoplastic suspension element method (VSEM) and viscoplastic divided space element method (VDEM), are proposed and some analytical results are shown in this paper. The deformation of fresh concrete in various consistency tests, such as slump and flow tests, and in various casting conditions is obtained theoretically, and the relationship between the behavior of fresh concrete in these conditions and the rheological constants is clarified. The adequacy of the analytical methods is examined by comparison with experimental results.

2. Viscoplastic Finite Element Method

2. 1 Outline of Analysis

(1) Constitutive Law of Fresh Concrete

The total strain rate $\{\dot{\varepsilon}\}$ of a viscoelastic material is given in the following equation when strain components due to temperature change can be negligible.

$$\{\dot{\varepsilon}\} = \{\dot{\varepsilon}^e\} + \{\dot{\varepsilon}^v\} = \frac{\{\dot{\varepsilon}^e\} + \{\sigma'\}}{2\eta_G} + \frac{\{\sigma_m\}}{2\eta_K} \tag{1}$$

in which $\{\dot{\varepsilon}^e\}$: elastic strain rate; $\{\dot{\varepsilon}^v\}$: viscous strain rate; $\{\sigma'\}$: deviatoric stress; $\{\sigma_m\}$: mean stress; η_G, η_K: coefficients of viscosity for shear and bulk strain, respectively.

It may be said that the elastic deformation of fresh concrete is very small in comparison with its viscous deformation, and the bulk strain is considered to be very small in comparison with the shear strain at flow. Consequently, the following simple constitutive equation is used in this analysis.

$$\{\dot{\varepsilon}\} = \frac{\{\sigma'\}}{2\eta_G} \tag{2}$$

It is well known that the properties of fresh concrete cannot be explained by an idealized model of Newtonian liquid, but that they can be approximately expressed by an idealized model of Bingham plastic solid[3], as shown in Fig. 1, in which the flow initiates when larger stress than a specified stress-deviation (yield stress) acts on it. The yield function proposed by Bingham expresses the behavior of viscoplastic material under a pure shear stress state. In this analysis, the following equation proposed by Hohenemser and Prager[6] for arbitrary stress state is used.

$$2\eta V_{ij} = \begin{cases} 0 & (F < 0) \\ F\sigma'_{ij} & (F \geqq 0) \end{cases} \tag{3}$$

The yield function F is expressed as $F = 1 - \tau_y/\sqrt{J_2}$ in which η: plastic viscosity; V_{ij}: tensor of strain rate; σ'_{ij}: tensor of deviatoric stress; τ_y: yield value; J_2: second invariant of the deviatoric stress tensor.

In the state of pure shear stress, Eq. 3 expresses the Bingham model as shown in Fig. 1. A material expressed by this constitutive law is incompressible, becomes rigid in a negative value of the yield function, and flows in a positive value.

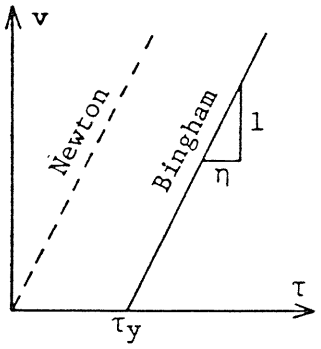

Fig. 1. Newtonian liquid and Bingham liquid.

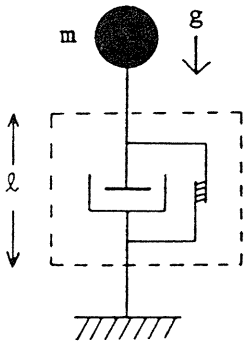

Fig. 2. Simple dumped system.

(2) Approximation of Dynamic Behavior

The force-strain rate relation of a simple damped system as shown in Fig. 2 (Bingham model) is expressed by

$$R = (\tau_y + \nu\eta)s \tag{4}$$

in which R: resisting force; ν: strain rate; s: area of section. In the condition of static equilibrium, the resisting force R is equal to the product of acceleration of load g and mass m.

$$\nu' = \frac{\frac{gm}{s} - \tau_y}{\eta} \tag{5}$$

in which ν′: strain rate in the condition of static equilibrium. If it moves with a constant velocity of ν′, the static equilibrium condition is maintained. The result obtained by the FEM analysis is the displacement rate in the static equilibrium condition. However, in the dynamic equilibrium condition, the equation of motion for this system is

$$gm - R = am \tag{6}$$

in which a: acceleration. Substituting Eq. 4 into Eq. 6 leads to a differential equation of motion, and the following equation is obtained by solving it.

$$\nu = C \exp(-Bt) + \frac{A}{Bl} \tag{7}$$

in which C: constant; $A = g - \tau_y s/m$; $B = \eta s/ml$; t: time; l: length of element. By substituting Eq. 5 and the strain rate ν_0 at $t = 0$ into Eq. 7, the strain rate ν is expressed as a function of time t.

$$\nu = (\nu_0 - \nu') \exp(-Bt) + \nu' \tag{8}$$

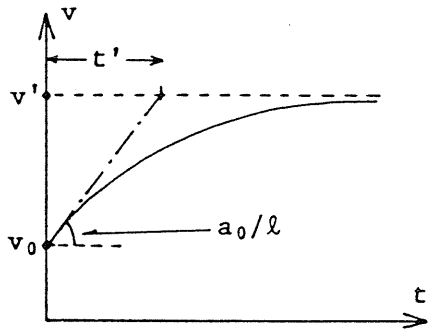

Fig. 3. Variation of strain rate.

Fig. 3 shows the variation of strain rate expressed by Eq. 8 from ν_0 to ν', and indicates the retardation of changing velocity. The acceleration a_0 at $t = 0$ is

$$a_0 = (\nu' - \nu_0)Bl = \frac{g - (\tau_y + \nu_0\eta)}{m} \tag{9}$$

As the parameter B is equal to the inverse of retardation time t' shown in Fig. 3, Eq. 8 can be expressed

$$\nu = (\nu_0 - \nu') \exp\left(\frac{-t}{t'}\right) + \nu' = (\nu' - \nu_0)\left[1 - \exp\left(\frac{-t}{t'}\right)\right] + \nu_0 \tag{10}$$

The retardation time t' is a function of plastic viscosity η and mass m, and the strain rate ν of an element is calculated with the strain rate ν_0 at the former step and the strain rate ν' in static equilibrium by setting up t' with a certain value. In the analysis, the calculation is repeated with the step of time Δt, and the average of strain ν^* in Δt is expressed by the following equation which is obtained by Eq. 10 and Δt.

$$\nu^* = \frac{(\nu_0 - \nu)t'}{\Delta t} + \nu' \tag{11}$$

(3) Method of Analysis

Fig. 4 shows the flow chart of the program for the analysis. The outline of the analysis is as follows: First, the elastic stress $\{\sigma^e\}$ of each element is obtained for external force, and the

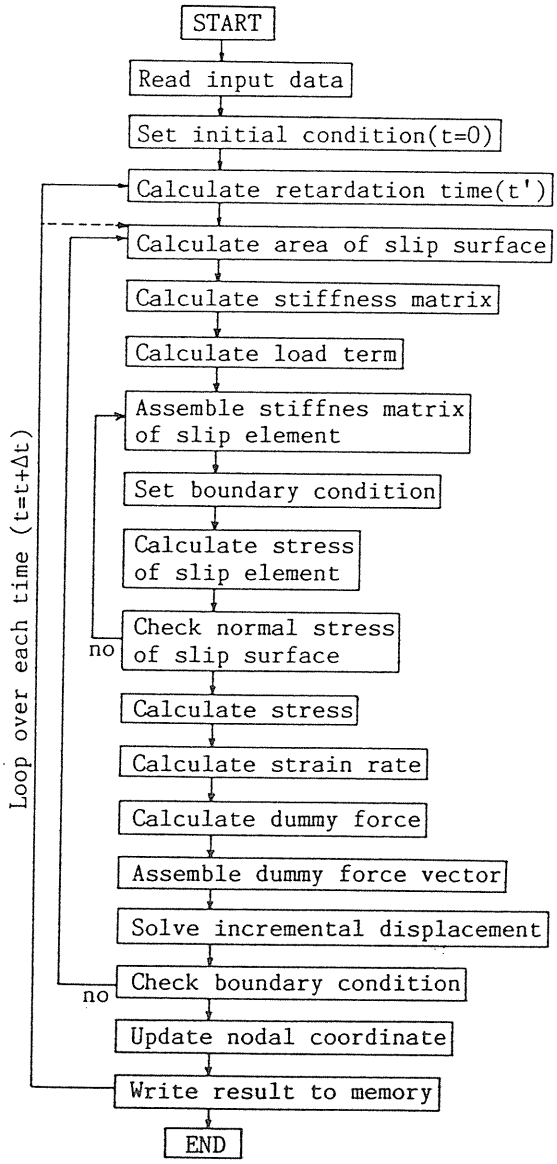

Fig. 4. Flow-chart of program for viscoplastic finite element method (VFEM).

strain rate $\{\dot{\varepsilon}\}$ is calculated with Eq. 3 and Eq. 11. Then the dummy elastic stress $\{\sigma^*\}$ is given from multiplication of $\{\varepsilon^e\}$ by elastic stiffness matrix D. The dummy force vector $\{F^*\}$ at each nodal point is calculated by integration for the dummy elastic stress $\{\sigma^*\}$. Next, the elastic calculation is carried out for this dummy nodal force $\{F^*\}$, and incremental displacement by viscosity is obtained. The shape of fresh concrete as it is flowing is given for every time by repetition of the above calculation at each time step.

(4) Slipping on Form Surface

When fresh concrete slips on the surface of a form, the resisting force acts in the reverse direction of displacement, which is related to cohesive stress and friction[7]. In case of axisymmetric problems, slipping resistance can be treated as nodal force. However, it becomes difficult to express the slipping resistance as that of a nodal force on the boundary surface in three-dimensional problems, because the direction of displacement by slipping on the boundary surface cannot be estimated before calculation.

In this analysis a slip element, consisting of a dashpot and a slider expresses the properties of a Bingham model, and spring elements are introduced in the practical as shown in Fig. 5(a). Therefore, the input data for describing the slipping behavior, i.e. the relationships between shear stress and strain rate, are essential. The rheological constants (yield value and plastic viscosity) of the slip element are expressed as a function of normal stress acting on the slip surface. This normal stress and acting area (called "slip area" in this paper) must be calculated at each step of calculating time. The model of slip area used in this analysis is shown in Fig. 6. in which the area is evaluated according to whether nodal points on the surface of concrete touch the surface of the form or not.

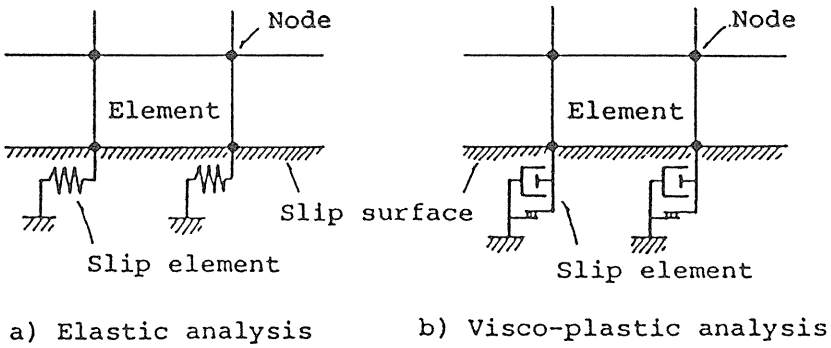

Fig. 5. Slip element.

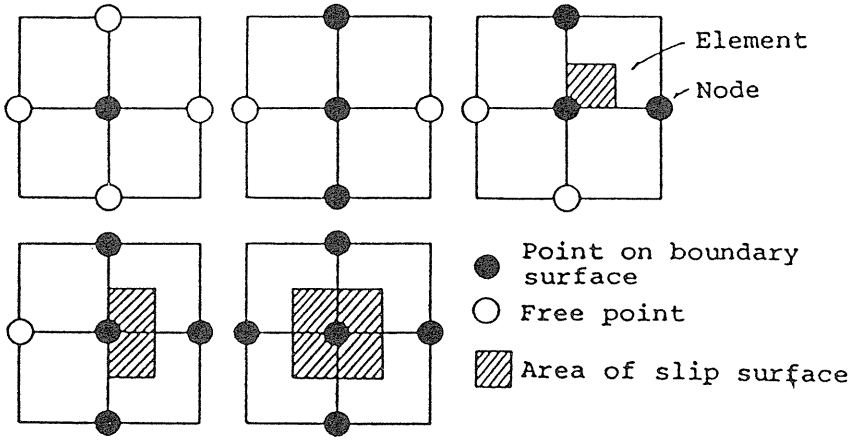

Fig. 6. Evaluation of slip area.

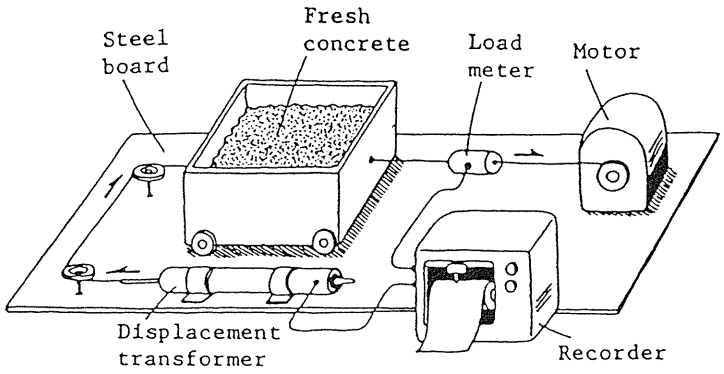

Fig. 7. Slipping resistance test.

An experiment was carried out to measure the fundamental properties of slipping resistance between fresh concrete and steel board. Wooden forms are generally used in practical concreting works, and the slipping resistance at the surface of wood differs from that at the surface of steel. Even for the same material, slipping properties may be affected by the surface condition. In this study, steel and acrylic board were used as the formwork, and smooth-faced steel board was used for the measurement of slipping resistance of fresh concrete. An apparatus for the slip test is shown in Fig. 7. In the experiment, the slipping resisting force was measured under three different normal stresses and three different slip velocities for each type of material. Some examples of experimental results are shown in Fig. 8. The slipping resisting force increases linearly as the slip velocity and the normal stress increase. The relationship between slipping resisting stress σ_h and slip velocity β can be expressed as a function of the slipping yield stress τ_a and the slipping viscosity η_s

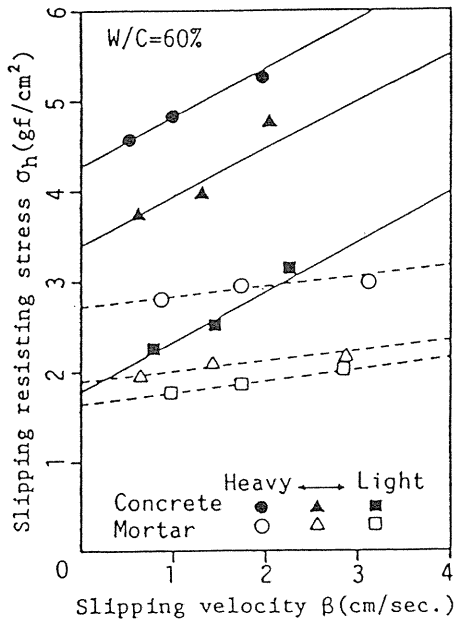

Fig. 8. Relationship between slipping resisting stress and slipping velocity.

$$\sigma_h = \tau_a + \eta_s \beta \tag{12}$$

As two parameters in Eq. 12 are affected by normal stress σ_n, the slipping stress is expressed by a function of slip velocity and normal stress as follows:

$$\sigma_h = S_1 \beta \sigma_n + S_2 \beta + S_3 \sigma_n + S_4 \tag{13}$$

The parameters S_1-S_4 in Eq. 13 can be determined from experimental results, and used in the following simulations.

2. 2 *Simulation of Slump Test*

(1) Method of Analysis

In the simulation of slump test, triangle axisymmetric element are used, and the finite element idealization is shown in Fig. 9. The input parameters are shown in Table 1. As the adhesive stress τ_h and the frictional coefficient μ that act on the slipping surface between fresh concrete and bottom steel board, the mean values ($\tau_h = 0.8$ gf/cm^2, $\mu = 0.15$) obtained from the experiment mentioned above are used. It was confirmed in the experiment that the effects of the adhesive stress and the frictional coefficient on the behavior of fresh concrete in the slump test are negligible. In this analysis, the arresting action of flowing caused by touching between slump cone and fresh concrete is considered.

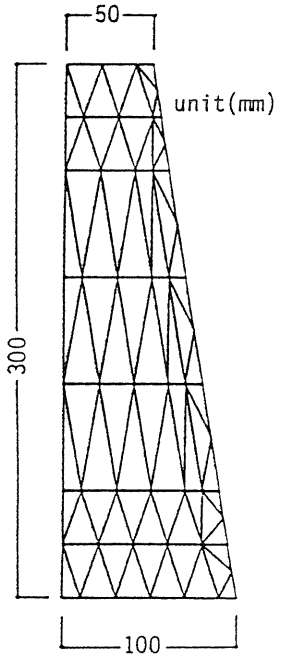

Fig. 9. Finite element idealization for simulation of slump test.

Table 1. Parameters of analysis for slump test and flow test.

Variable parameters

Specific gravity ρ		Plastic viscosity η(kPa·s)		Yield value τ_y(gf/cm^2)	
value	mark	value	mark	value	mark
3.0	h	0.04	04	2	1
		0.06	06	4	2
		0.10	10	6	3
2.2	n	0.14	14	8	4
		0.18	18	10	5
		0.22	22	12	6
		0.26	26	14	7
1.8	l	0.30	30	16	8
				18	9

series name

Simulation

test	mark
slump flow	s f

Constant parameters

Adhesive force τ_h(gf/cm^2)	Frictional coefficient μ
0.8	0.15

(2) Analytical Results and Discussion

An example of the analytical results of the flowing of fresh concrete after lifting of the slump cone (that is called "slumping") is shown in Fig. 10. Observing the shape of fresh concrete after slumping, a dent at the top surface and discontinuous slope at the middle of the side surface (that is made by the touch of the slump cone) are seen clearly. These phenomena can be observed experimentally as shown in Photo. 1.

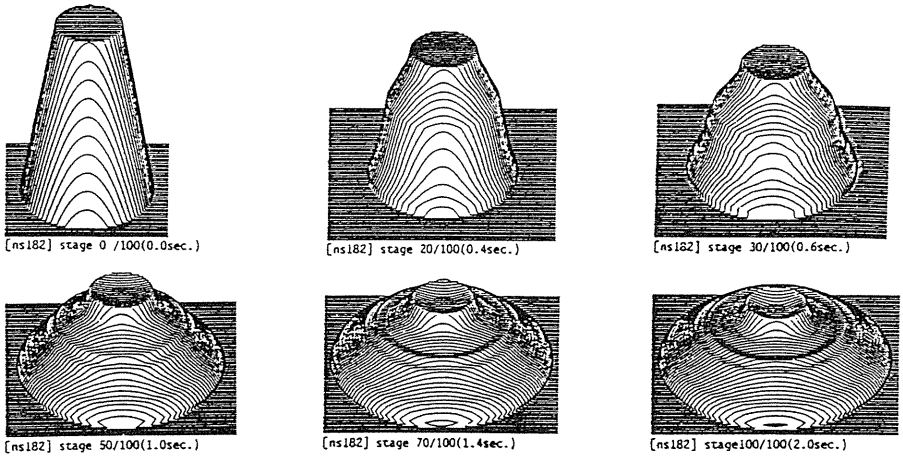

Fig. 10. Example of analytical results of slump test.

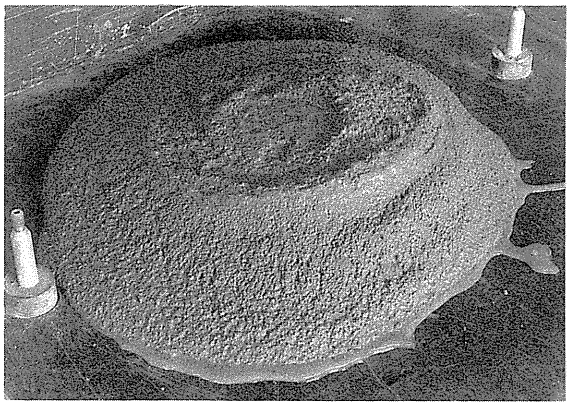

Photo. 1. Slump test of mortar.

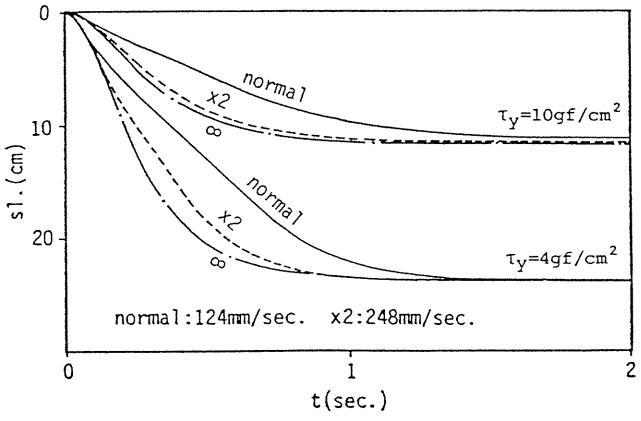

Fig. 11. Effect of lifting velocity of slump cone on slumping(sl.) — time(t) curves.

Fig. 11 shows the effect of the velocity of lifting of the slump cone on slumping sl. – time t curves. At the beginning of lifting of the slump cone, its inner surface arrests the flowing of fresh concrete, and the velocity of lifting of the slump cone controls the flowing velocity of fresh concrete. However, the slump value, that is the height of fresh concrete at the end of slumping, is hardly affected by the velocity of lifting of the slump cone. Fig. 12 shows the effect of yield value τ_y on the sl. – t curves. According to the analytical results, the slump value of normal weight concrete will be 0 cm if the yield value becomes larger than about 20 gf/cm^2.

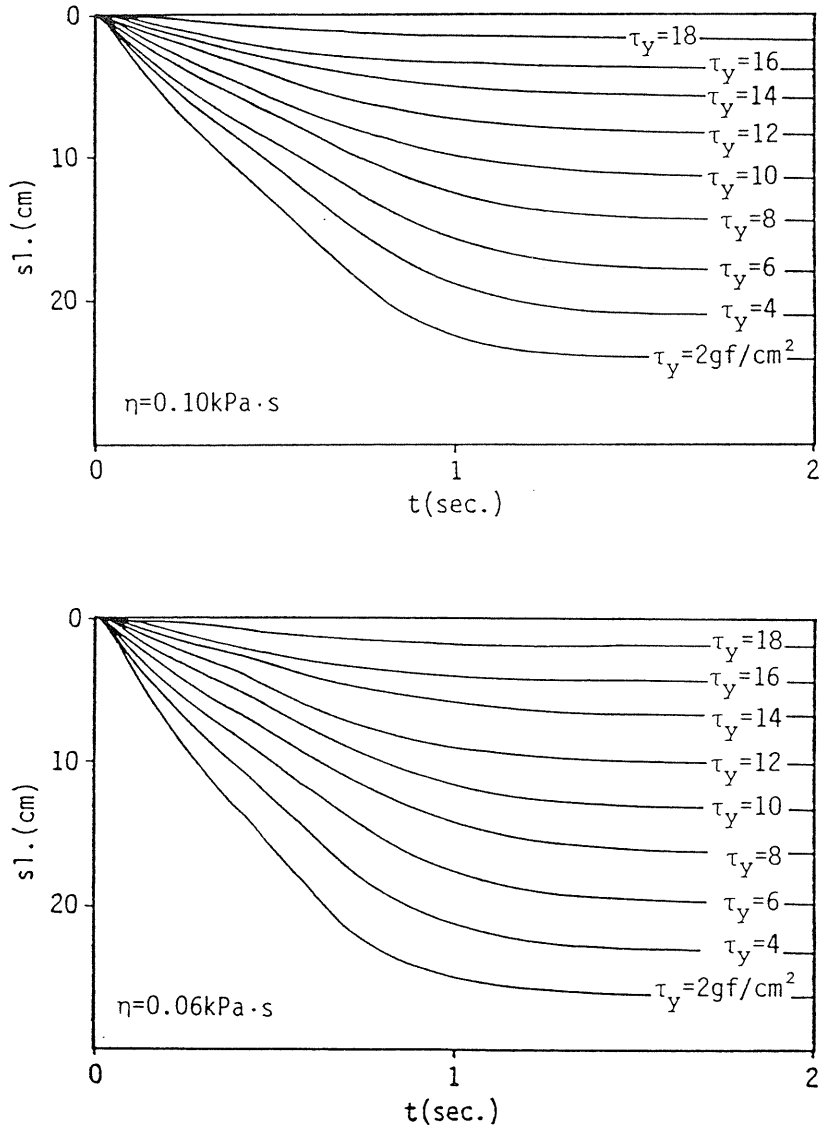

Fig. 12. Effect of yield value (τ_y) on slumping(sl.) – time(t) curves.

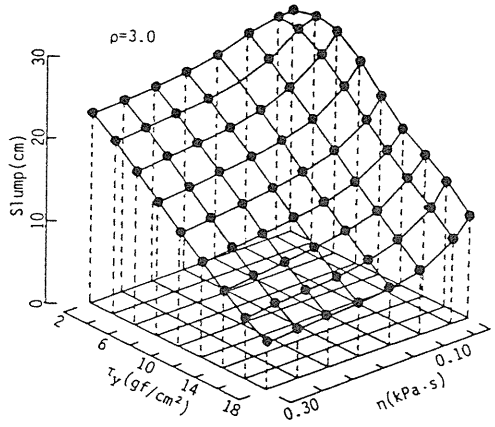

(a) Heavy weight concrete

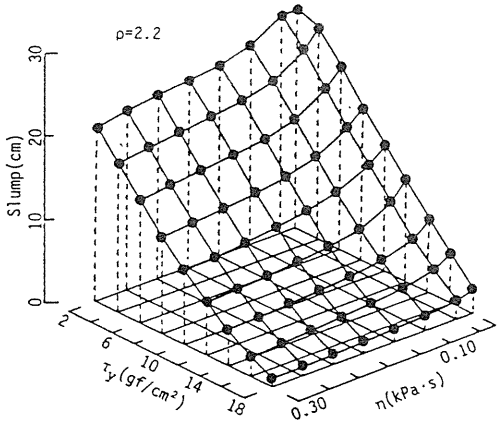

(b) Normal weight concrete

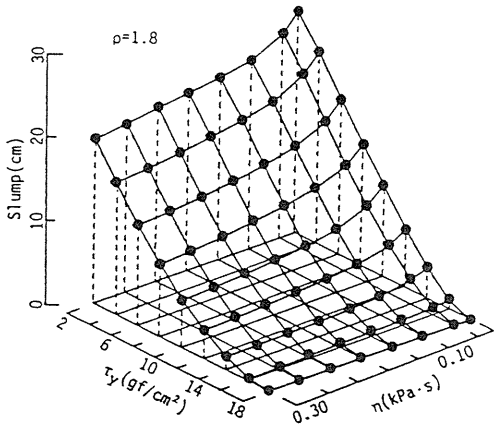

(c) Lightweight concrete

Fig. 13. Effect of rheological constants (τ_y, η) on slump value(Sl.).

Fig. 13 shows the effects of the two rheological constants, i.e., yield value τ_y and plastic viscosity η, on the slump value Sl. The three sections of Fig. 13 show the simulated results for the specific gravities of 3.0, 2.2 and 1.8, corresponding to heavy weight, normal weight and lightweight fresh concretes or mortars, respectively. As shown in these figures, the slump value Sl. increases with decreasing yield value τ_y and plastic viscosity η, and it is more sensitive to the yield value than the plastic viscosity.

2. 3 Simulation of Flow Test

(1) Method of Analysis

The flow test stipulated in JIS R 5201 is simulated by VFEM. The finite element idealization and the input parameters are shown in Fig. 14 and Table 1, respectively. The method of analysis is the same as that of the slump test, but the impact force by drop of the flow table is necessary to consider in the simulation of flow test. In this analysis, the impact force by drop is translated to the acceleration acting equally on all nodal points and it is assumed that the potential energy lost by drop of 1 cm of the flow table is consumed for the deformation of fresh mortar. Therefore the acceleration is calculated iteratively based on the condition that the sum of the product of force and displacement is equal to the potential energy. The acceleration increases as the fluidity decreases and the shape of fresh mortar deformed by drop becomes flat. This analytical method is different from the earlier one[8], which assumes that a constant acceleration acts on fresh mortar in the flow test.

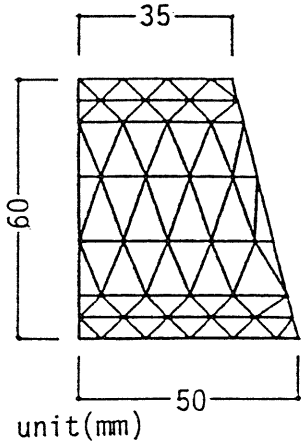

Fig. 14. Finite element idealization for simulation of flow test.

(2) Analytical Results and Discussion

An example of the analytical results of the flowing of fresh mortar is shown in Fig. 15. In this figure, a dent at the top surface is seen as in the simulation of slump test, but the outline of the top surface tends to spread finally as shown in Photo. 2. The effects of the rheological constants on the relationship between flow value fl. and number of drops n are shown in Fig. 16. The fresh mortar deforms before drop of the flow table when the yield value is less than about 4 gf/cm^2 in the analysis. The flow value − drop number curves tend to become more

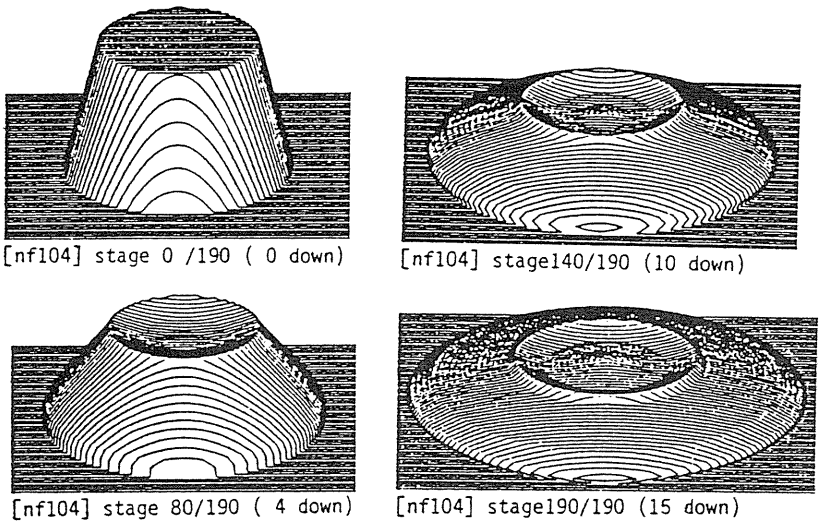

Fig. 15. Example of analytical results of flow test.

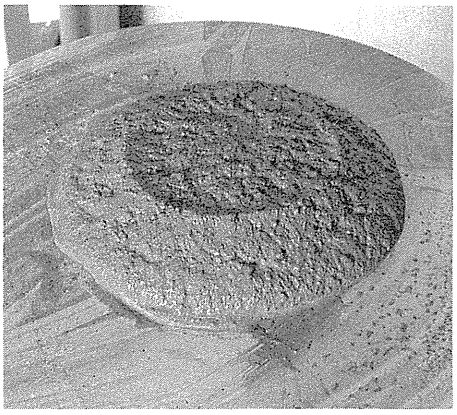

Photo. 2. Flow test of mortar.

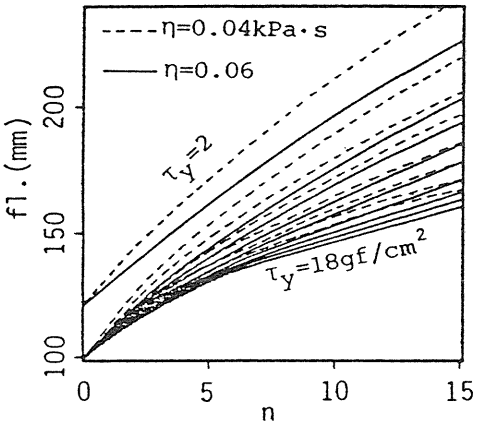

Fig. 16. Effect of theological constants (τ_y, η) on flow value(fl.) — drop number(n) curves.

nearly linear with increasing plastic viscosity and more curved at the latter portion with increasing yield value. The effects of the yield value τ_y and plastic viscosity η on the flow value Fl. after 15 drops are shown in Fig. 17. In the figure, the differences between the flow value before drop of the flow table and that after 15 drops (Fl.15—Fl.0) are plotted on the vertical axis. As shown in Fig. 17, the flow value increases with decreasing yield value τ_y and plastic viscosity η. In comparison with the slump value (see Fig. 13), the flow value is more affected by the plastic viscosity. As the yield value and the plastic viscosity become large, however, the flow value is less affected by the rheological constants.

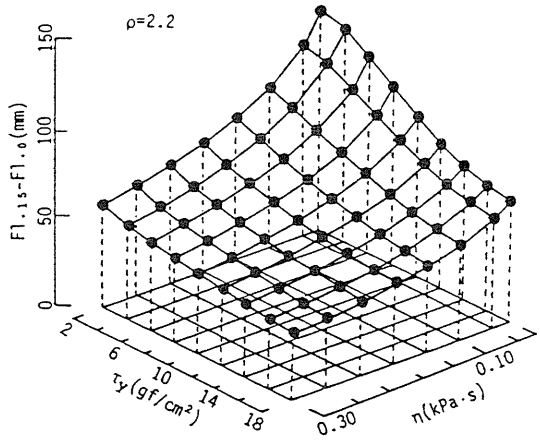

Fig. 17. Effect of rheological constants (τ_y, η) on flow value(Fl.).

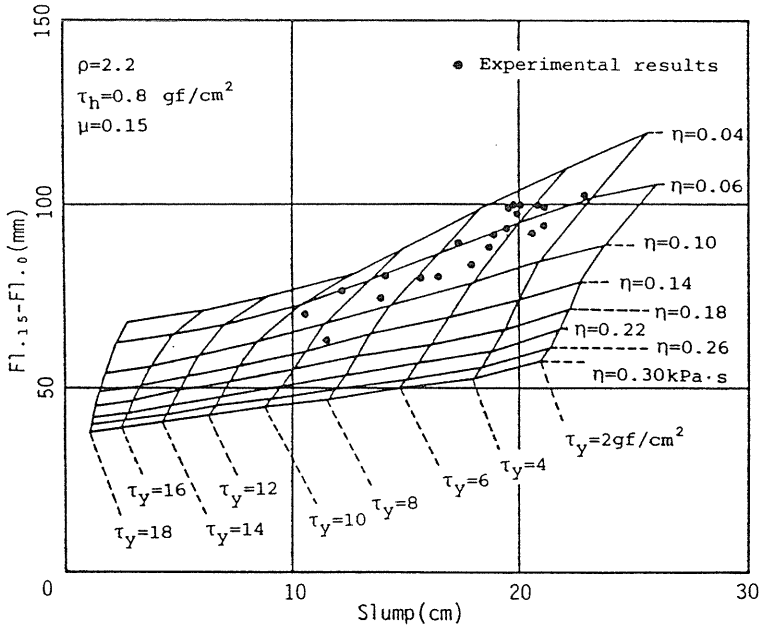

Fig. 18. Estimation of yield value(τ_y) and plastic viscosity(η) by slump and flow values.

2. 4 *Examination of Analytical Method*

Fig. 18 shows the relationship between slump value and flow value obtained by the analysis using various input data of rheological constants. If the experimental values obtained by the slump test and the flow test are both available for the same sample, two rheological constants can be estimated by using this figure. In Fig. 18, the horizontal axis expresses the slump value, and the vertical axis the amount of variation of flow value by 15 drops.

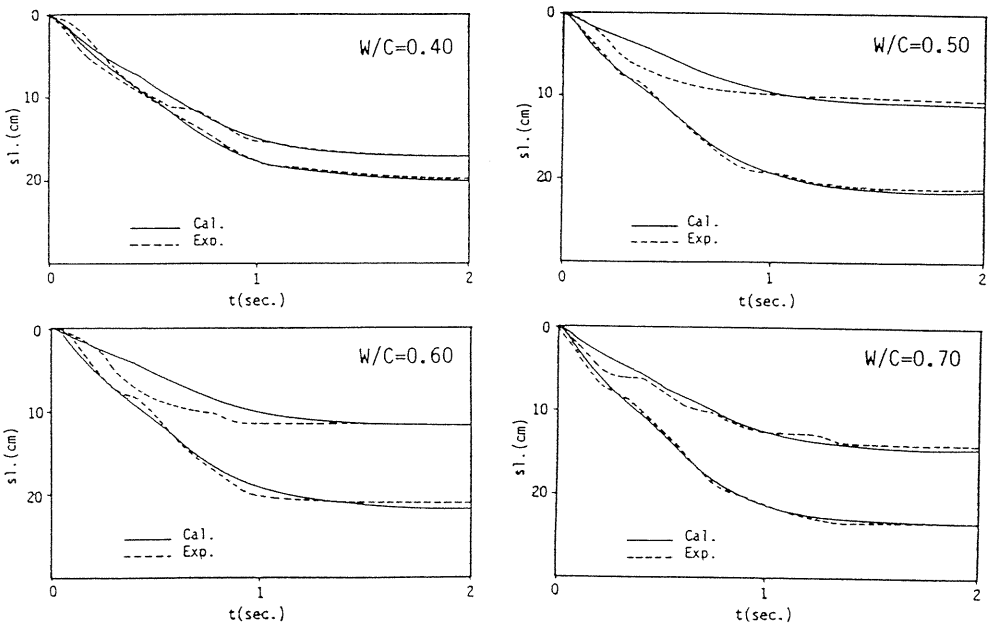

Fig. 19. Comparison between analytical and experimental slumping(sl.) — time(t) curves.

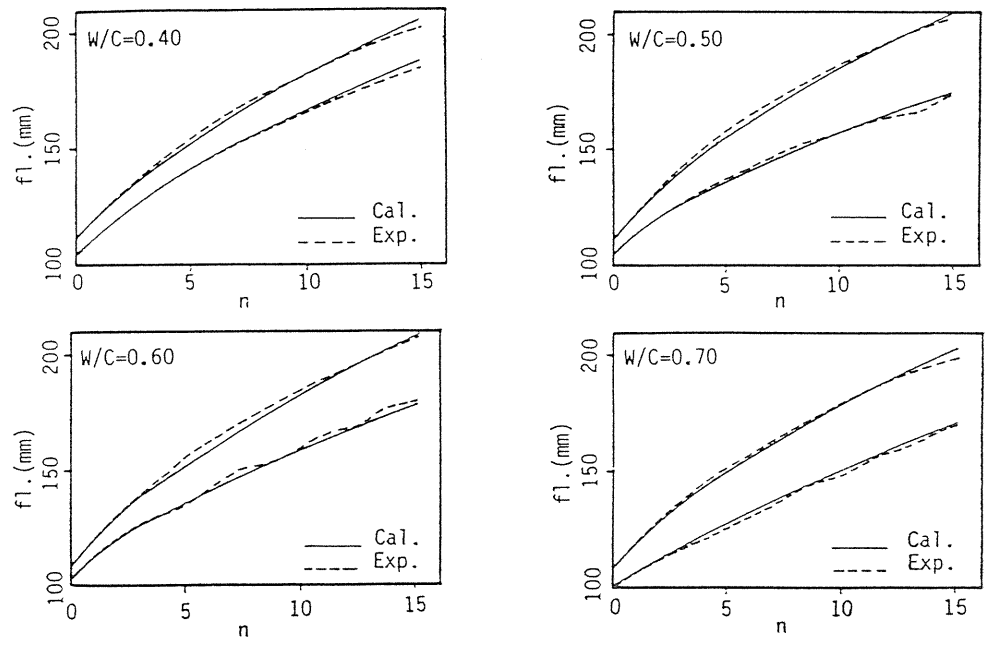

Fig. 20. Comparison between analytical and experimental flow value(fl.) — drop number(n) curves.

For comparison with analytical and experimental slumping sl. – time t curves or flow value fl. – number of drops n curves, the value of rheological constants of fresh mortar obtained by using Fig. 18 are used as input data of the analysis. The results are shown in Fig. 19 or Fig. 20. The analytical curves are comparable with the experimental curves in all series. According to the slumping sl. – time t curves shown in Fig. 19, the experimental curves give a lower slump value than the analytical curves at the portion that the time t is small. This may have resulted from the fact that the rheological properties of fresh concrete differ at the upper portion from the lower one in a slump cone. When fresh concrete is compacted in a slump cone by tamping rod, concrete in upper portion flows more easily or has a smaller yield value and plastic viscosity than in the low portion. It is considered that the falling of the upper portion occurs at the beginning of lifting of the slump cone, and that the irregular sl. – t curves mentioned previously are measured. This tendency is more remarkable in concrete with lower slump value. It is necessary to study the difference of the rheological properties of fresh concrete between the upper and lower portions in the slump cone.

2. 5 Simulation of Cylindrical Rotation Viscometer

The cylindrical rotation viscometer is one of the most general apparatus to measure the rheological constants of viscous materials[9,10]. However, it is pointed out that the application of this test method to composite materials such as fresh concrete including large aggregates is limited because it has been developed for homogeneous materials[11]. Therefore, the results of fresh concrete obtained by this method in each laboratory are considerably scattered due to the difference of each testing condition, size and shape of apparatus, etc.

In applying the cylindrical rotation viscometer to measure the rheological properties of fresh concrete, the following problems should be fully examined:

1) The laminar flow can not be assumed because the size of aggregates is relatively large comparing with that of apparatus.
2) It is necessary to consider the slip at the surface of rotor because the yield value of concrete is large.
3) The influence of the torque absorbed at the bottom surface of inner rotor is not clear.
4) As the self weight of fresh concrete in the lower portion of apparatus is large than that in the upper portion, it may be more difficult to flow in the lower portion due to the interlocking of aggregates (internal friction), but this phenomenon has never been clarified.

The purpose of this simulation is to investigate the problems mentioned above by VFEM analysis. In this paper, the influence of the slip at the surface of rotor (problem 2) is mainly examined, and the effects of the conditions such as the size and shape of apparatus, the internal friction of material and the torque absorbed at the bottom surface of apparatus on the measured rheological constants of fresh concrete are discussed.

(1) Method of Analysis

For the simulation of cylindrical rotation viscometer, axisymmetric ring elements are used. Stress and strain in circumferential direction should be considered as a three-dimensional problem. The coordinate system and strain matrix used in the analysis are shown in Fig. 21 and Table 2, respectively. The analysis is not different from the ordinary three-dimensional one with the exception of an assumption that the components of stress and displacement are all equal in circumferential direction θ.

In the cylindrical rotation viscometer, the inner and outer rotors move relatively in θ-direction, and the torque is transferred to the materials which touch to the surface of rotor by slipping resistance force. To consider the relative movement of the material and rotor, slip elements and slip area models proposed earlier are used in the analysis. The outline of the

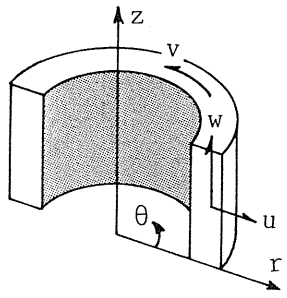

Table 2. Axisymmetric strain matrix.

$$\{\varepsilon\} = \begin{Bmatrix} \varepsilon_r \\ \varepsilon_\theta \\ \varepsilon_z \\ \gamma_{\theta z} \\ \gamma_{zr} \\ \gamma_{r\theta} \end{Bmatrix} = \begin{Bmatrix} \partial u/\partial r \\ u/r \\ \partial w/\partial z \\ \partial v/\partial z \\ \partial u/\partial z + \partial w/\partial r \\ \partial v/\partial r - v/r \end{Bmatrix}$$

Fig. 21. Analytical coordinate system.

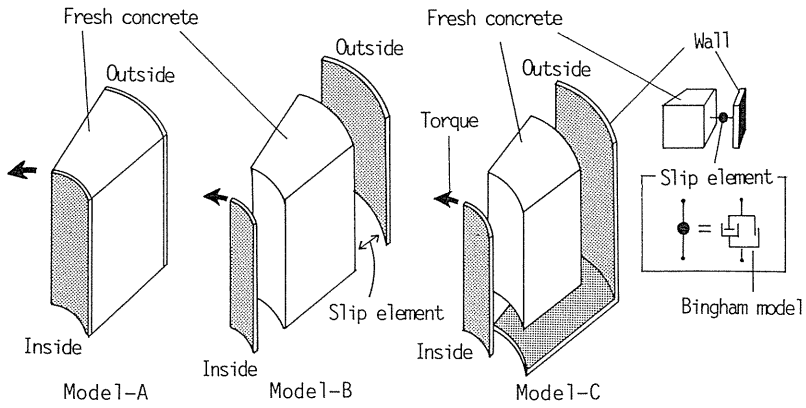

Fig. 22. Analytical models for simulation of rotation viscometer.

analytical model is shown in Fig. 22. In this figure, Model-A is an ideal model, where no slip occurs at the surface of rotor and no resistance at the bottom surface. In Model-B, both sides of rotors are fixed with slip elements, but no resistance occurs at the bottom surface to observe the slipping behavior. In Model-C, friction force at the bottom surface is introduced by slip elements. The slip resisting behavior measured by an experiment is used as input data in the analysis.

The finite element idealization used in the simulation is shown in Fig. 23. In this analysis, the torque is applied on the inner rotor in θ-direction. The rheological properties of fresh concrete and the shape of cylindrical rotation viscometer used in this analysis are shown in Table 3 and Table 4, respectively.

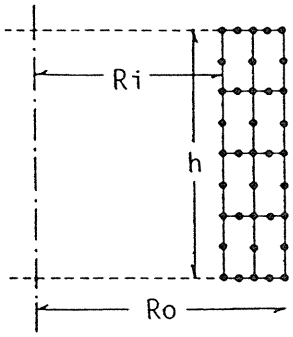

Fig. 23. Finite element idealization.

Table 3. Rheological properties of fresh concrete.

τ_y(gf/cm^2)	η(kPa•s)	tanϕ	ρ	S_1	S_2	S_3	S_4
0.0∿3.0	0.06∿0.10	0.0∿0.3	2.3	0.03	0.10	0.06	1.60

[Notes] τ_y:Yield value, η:Plastic viscosity, tanϕ:Internal frictional coefficient, ρ:Specific gravity, S_1∿S_4:Parameters of slipping resistance in following equation; $\sigma_h=S_1\beta\sigma_n+S_2\beta+S_3\sigma_n+S_4$, σ_h:Slipping resistance stress(gf/cm^2), β:Slipping velocity(cm/sec.), σ_n:Normal stress (gf/cm^2).

Table 4. Size of apparatus.

h	Ro	Ri/Ro
20.0∿35.0	10.0∿25.0	0.1∿0.9

[Notes]
h :Height of inner cylinder (cm)
Ri:Radius of inner cylinder (cm)
Ro:Radius of outer cylinder (cm)

(2) Analytical Results and Discussion

An example of the analytical results for Model-A is shown in Fig. 24. This figure shows the consistency curves plotted with strain rate $\dot{\gamma}$ and shear stress τ that are calculated from torque M of input value and angular velocity of rotor Ω of output value by using Eq. (1)

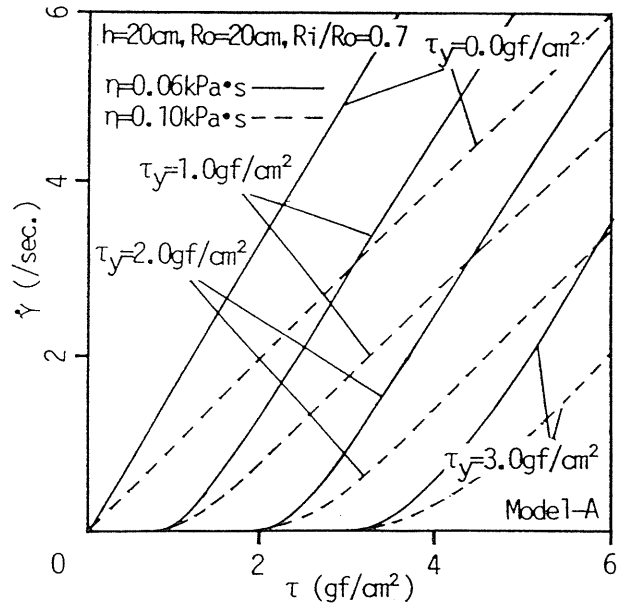

Fig. 24. Examples of analytical results (Model-A).

and Eq. (2) in Table 5. In this model with no slip at the surface of rotor, the plastic viscosity η^*, which is represented by inverse slope obtained from the linear part of later portion of the consistency curve, is exactly equal to input value η. And the yield value τ_y^*, which is obtained by Eq. (3) in Table 5 using the value of cross point on the τ-axis and extending the linear part of the consistency curve, almost coincides with input value τ_y. That is, the analytical results obtained, for the cylindrical rotation viscometer under an ideal condition are in good agreement with the theoretical ones. Thus it may be said that the applicability of this analytical method was examined.

Table 5. Equations of rotation viscometer.

$$\tau = \frac{M}{2\pi Ri^2 h} \quad -(1)$$

$$\dot{\gamma} = \frac{2\Omega}{1-(Ri/Ro)^2} \quad -(2)$$

$$\tau_y = \frac{(Ri/Ro)^2-1}{2\ln(Ri/Ro)} \cdot \tau_a \quad -(3)$$

where,
τ :Shear stress (gf/cm^2)
M :Torque (g•cm)
Ri:Radius of inner rotor (cm)
Ro:Radius of outer rotor (cm)
h :Height of inner rotor (cm)
$\dot{\gamma}$:Strain rate (/sec.)
Ω :Angular velocity of rotor (rad/sec.)
τ_y:Yield value (gf/cm^2)
τ_a:Intersection of stress axis and linear portion of consistency curve (gf/cm^2)

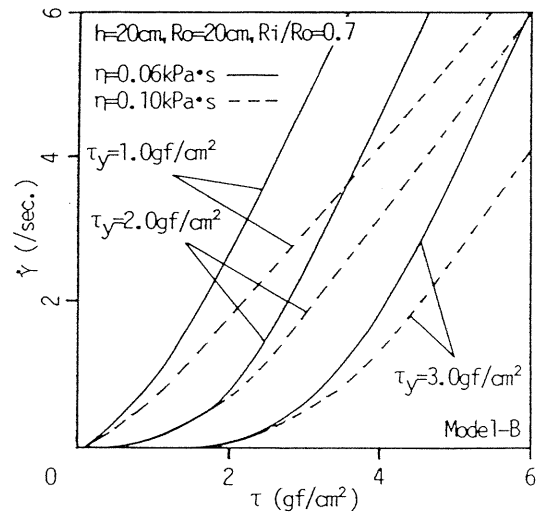

Fig. 25. Examples of analytical results (Model-B).

An example of the consistency curves obtained by Model-B which has slip elements at the surface of rotors is shown in Fig. 25. In general, the rotational velocity increases at the same torque, and the consistency curve moves to upper portion when the slip occurs between rotor and material. Therefore, the plastic viscosity and the yield value are measured as smaller than true values. As shown in Table 6 for example, this error of measurement caused by slip is affected by the rheological properties of material and the shape of apparatus.

Table 6. Comparison between input data and analytical results.

Input		Calculated (No Slipping)				
τ_y	η	τ_a*	τ_y*	η*	τ_y*/τ_y	η*/η
1.0	0.06	0.9(1.2)	0.68(0.91)	0.045(0.06)	0.68(0.91)	0.75(1.00)
2.0	0.06	2.1(2.5)	1.60(1.90)	0.042(0.06)	0.80(0.95)	0.70(1.00)
3.0	0.06	3.4(3.9)	2.58(2.96)	0.043(0.06)	0.86(0.99)	0.72(1.00)
1.0	0.10	1.2(1.2)	0.91(0.91)	0.072(0.10)	0.91(0.91)	0.72(1.00)
2.0	0.10	1.8(2.5)	1.37(1.90)	0.071(0.10)	0.69(0.95)	0.71(1.00)
3.0	0.10	3.2(3.9)	2.43(2.96)	0.067(0.10)	0.81(0.99)	0.67(1.00)

[Notes] τ_y:Yield value (gf/cm^2), η :Plastic viscosity (kPa•s), τ_a:Intersection of stress axis and linear portion (gf/cm^2).

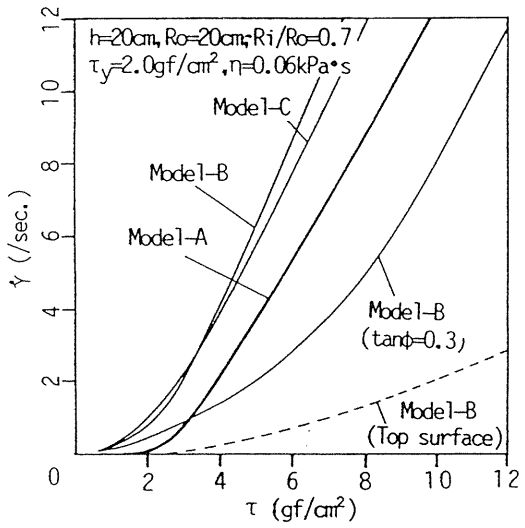

Fig. 26. Consistency curves of analytical models.

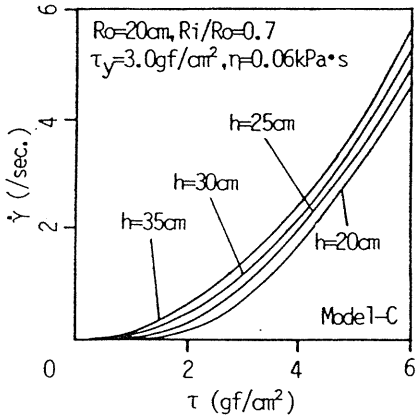

Fig. 27. Effect of height of apparatus (Model-C).

The comparison of the consistency curves for three models is shown in Fig. 26. In earlier studies[11], to make the influence of the resistance at the bottom portion smaller, another soft material was set at the bottom portion, or theoretical corrections were carried out. In this study, such modification is not applied. As shown in Fig. 26, however, the effect of the torque absorbed at the bottom surface is smaller than that of slip at the surface of rotor even in the extreme case of Model-C. Fig. 27 shows that the higher the height of cylinder makes the smaller the effect of the resistance at the bottom surface.

The internal friction due to the interlocking by aggregates occurs in fresh concrete and mortar. A simulation was carried out by using Model-B with the constitutive law proposed by the authors[12] which expresses the rheological properties depending on stress states. Fig. 28 shows an example of the analytical results. It is shown in this figure that the increase of the

internal friction (tanϕ) makes the consistency curves considerably lower, and causes larger error in measured curves. Fig. 29 shows that this tendency becomes remarkable with increasing height of cylinder. Therefore, it is not rational to use the higher cylinder to eliminate the effects of slip at the surface of rotor because of torque absorbed at the bottom surface.

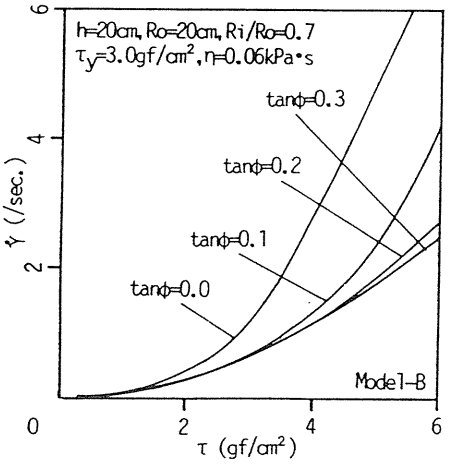

Fig. 28. Effect of internal friction (tanϕ).

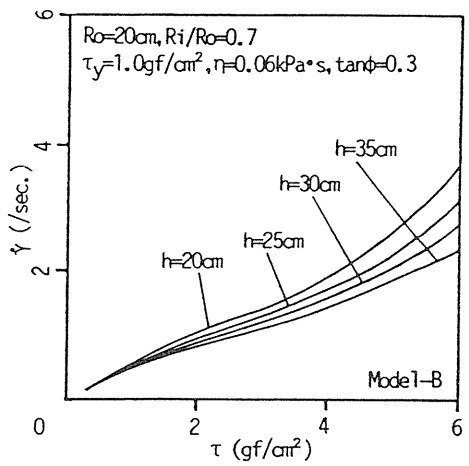

Fig. 29. Effect of height of apparatus (h).

The analytical results of the internal distribution of flow velocity in the cylindrical rotation viscometer are shown in Fig. 30 and Fig. 31. According to these figures, the flow velocity of material is not equal in the upper and lower portions. If the flow is arrested at the bottom surface, it becomes lower at the lower portion. Further, considering the internal friction of material, the flow velocity becomes smaller at the lower portion.

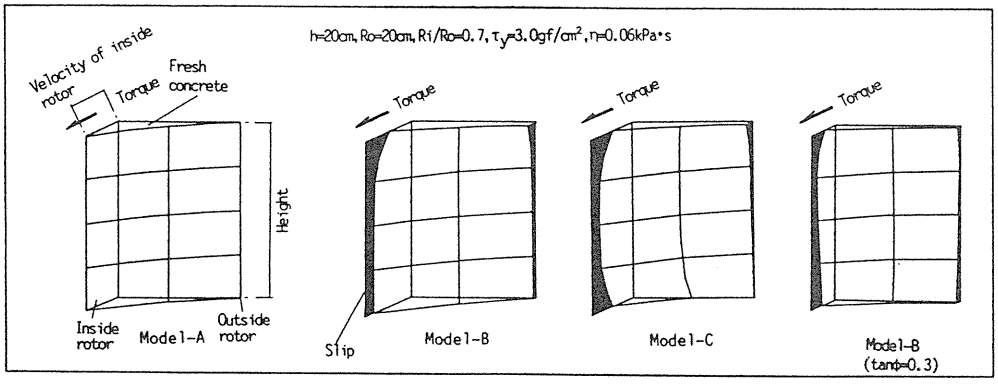

Fig. 30. Internal distribution of flow velocity (Comparison of analytical results by each model).

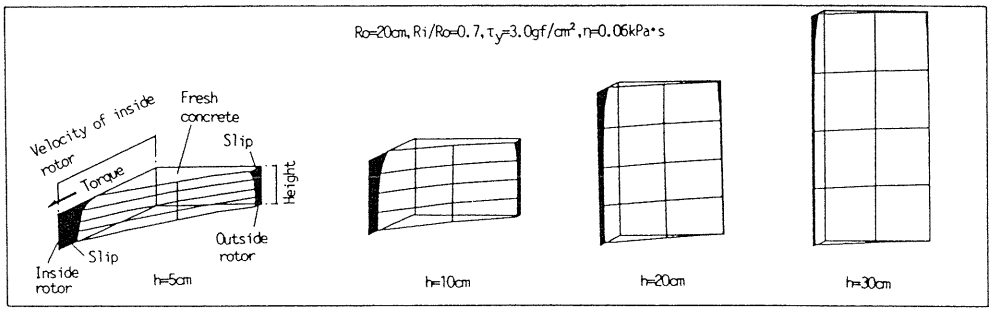

Fig. 31. Internal distribution of flow velocity (Effect of height of apparatus).

2. 6 *Simulation of Vibrating Slump Test*

(1) Method of Analysis

The consolidation of fresh concrete is generally performed by high frequency vibration. To examine the effects of various parameters related to vibrating force, such as acceleration, direction and frequency, on the flow properties of fresh concrete, the slump test subjected to vibration shown in Fig. 32 was used as a simple example.

Vibrating acceleration is introduced as nodal force, which is reversed reciprocally step by step because this is the simplest method of calculation. Large forces act in momentary time, and some elements of fresh concrete yield and flow. Even if the direction of vibration is horizontal, reciprocal force makes the concrete flow down in the direction of weight. Thus it is observed that the rheological constants of fresh concrete subjected to vibration become small. Furthermore, the normal stress acting on slip area of the form surface varies in response to the vibrating acceleration, and the slipping resistance decreases when the normal stress becomes small.

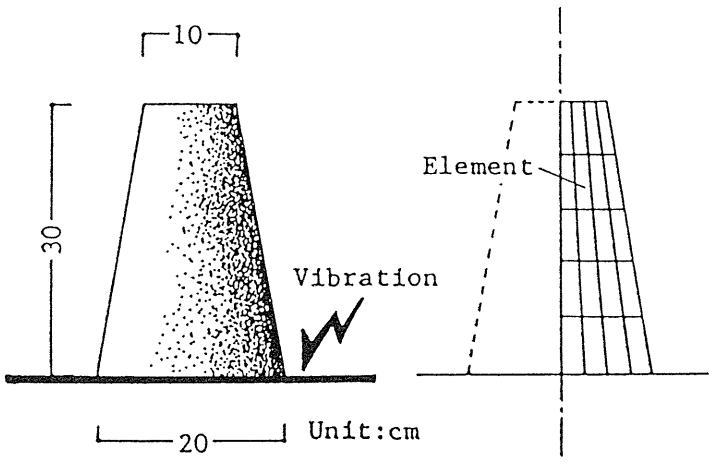

Fig. 32. Analytical example and finite element idealization for simulation of slump test subjected to vibration.

Earlier studies to measure the rheological properties of fresh concrete subjected to vibration report that the rheological constants become small due to structural failure[13]. However, it is impossible to measure accurately the properties of concrete under vibration, except for the effects of the contact of concrete with the surface of a vessel and the internal distribution of the vibrating force. In this analytical method, the effect of vibration can be estimated using the data obtained in the static state.

(2) Analytical Results and Discussion

Fig. 33 shows typical examples of the results of this simulation — the longitudinal axis represents the falling of the top surface of fresh concrete in the slump cone (slumping); the lateral axis represents the time after lifting of the slump cone. As shown in Fig. 33, the velocity of slumping and slump value (at the end of slumping) increase with increasing acceleration of vibration from 1g to 4g. The yield value τ_y of 20 gf/cm^2, used as one of the input data to obtain the analytical result in Fig. 33, corresponds to the value of zero slump concrete.

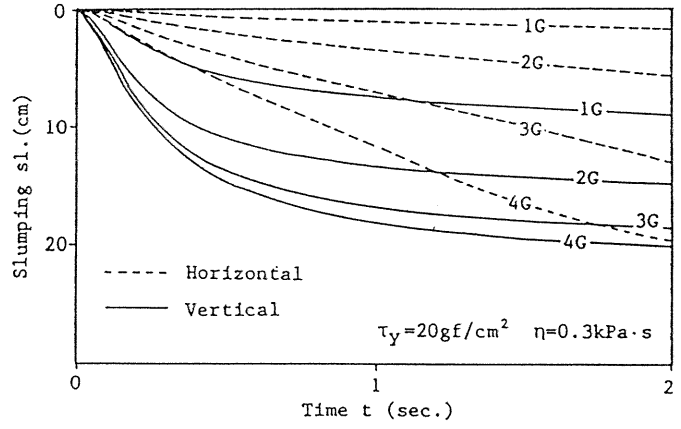

(a) η = 0.3 kPa·s

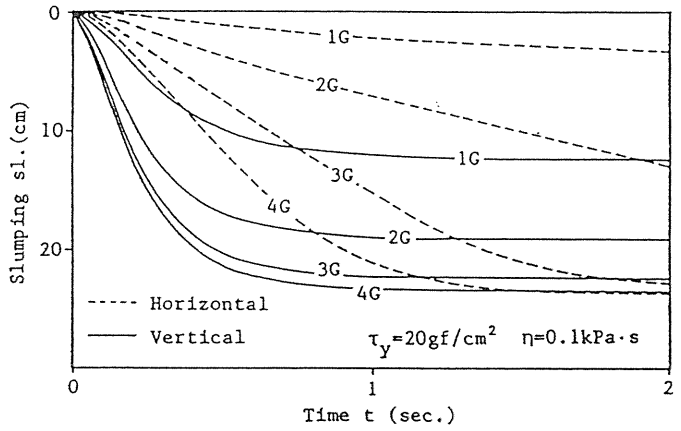

Fig. 33. Effect of acceleration and direction of vibration on slumping(sl.) — time(t) curves.

By acceleration of 4g, such dry mixed concrete behaves like wet mixed concrete whose slump value is 20 cm. The flowing speed of fresh concrete subjected to vertical acceleration is higher than that for horizontal acceleration, but the slump value at the end of slumping is hardly affected by the direction of acceleration. The effect of vibration on the plasticizing of concrete increases with decreasing plastic viscosity η independently of the direction of acceleration. It is well known that the yield value of fresh concrete generally becomes small with admixing of superplasticizer, and the plastic viscosity hardly changes. Consequently, the plastic viscosity of superplasticized concrete is much larger than that of normal concrete of the same slump value. The slump value is mainly related to the yield value only, according to the simulation result mentioned above, and the difference of plastic viscosity between normal and superplasticized concrete is not indicated clearly by the slump test. This analytical result, however, shows the considerable effect of plastic viscosity on the behavior of fresh concrete subjected to vibration, and it is necessary to establish a rational method for evaluating the consistency of fresh concrete such as superplasticized concrete.

Fig. 34 shows the effect of vibration on the relationship between the yield value and the slump value. As shown in this figure, concrete of slump value larger than 5 cm generally behaves like that of slump value 25 cm, by a comparatively small acceleration of 2g. The effect of frequency of vibration on the slumping – time curve is shown in Fig. 35. The velocity of flowing becomes slightly greater with decreasing frequency, but the frequency of vibration has no effect on the behavior of fresh concrete in the frequency range 25–100 Hz at the same acceleration. If the amplitude of vibration is constant, the frequency is increased because of increasing acceleration.

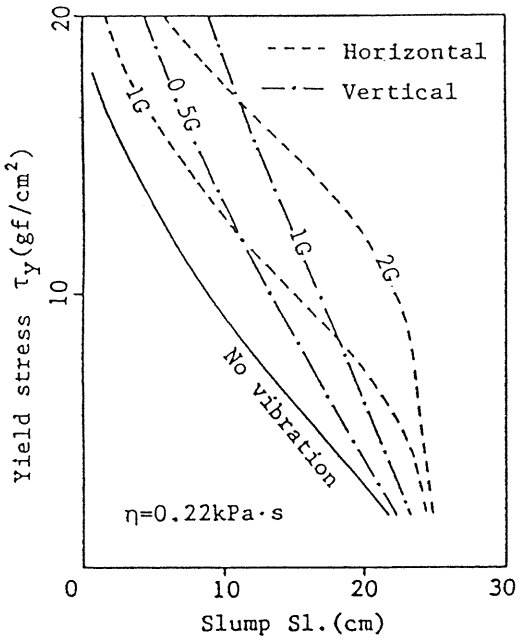

Fig. 34. Effect of acceleration and direction of vibration on relationship between yield value(τ_y) and slump value(Sl.).

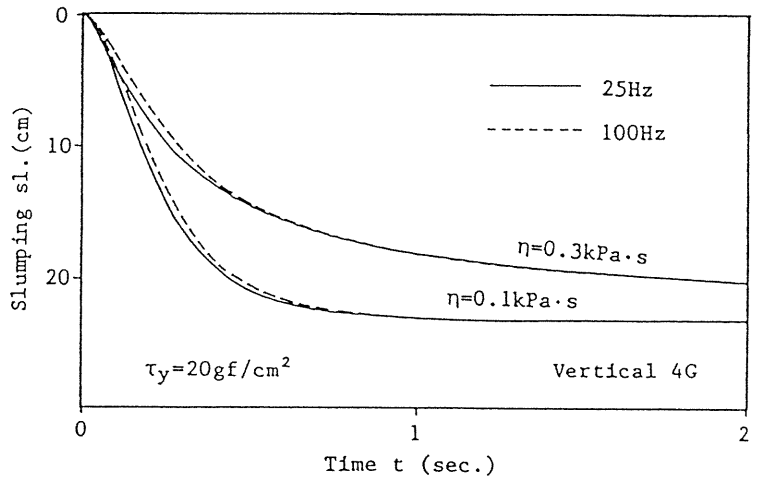

Fig. 35. Effect of frequency of vibration on slumping(sl.) – time(t) curve.

2. 7 *Simulation of Vibrating Consistency Test*

An example of analysis and idealization for the finite element method is shown in Fig. 36; the analytical results are shown in Fig. 37 and Fig. 38. The maximum acceleration in the standard vibrating consistency test is 1g (the amplitude is 0.8 mm and the frequency is 25 Hz). In the simulation, however, fresh concrete of slump value 3 cm ($\tau_y = 16$ gf/cm^2, $\eta = 0.2$ kPa · s) does not become flat in the vessel when it is subjected to vertical acceleration of less than 3g, as shown in Fig. 38. It is thought that the disagreement results from ignoring the segregation due to vibration in the analysis, and the simulation method cannot be applied for the analysis of bleeding or rising of mortar and paste in fresh concrete. The upper portion of fresh concrete in the apparatus becomes comparatively flowable under vibration. This means that the two rheological constants of fresh concrete in the upper portion are smaller than those in the lower portion.

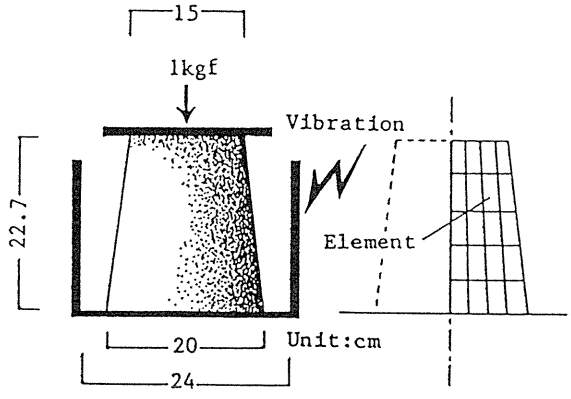

Fig. 36. Analytical example and finite element idealization for simulation of vibrating consistency test.

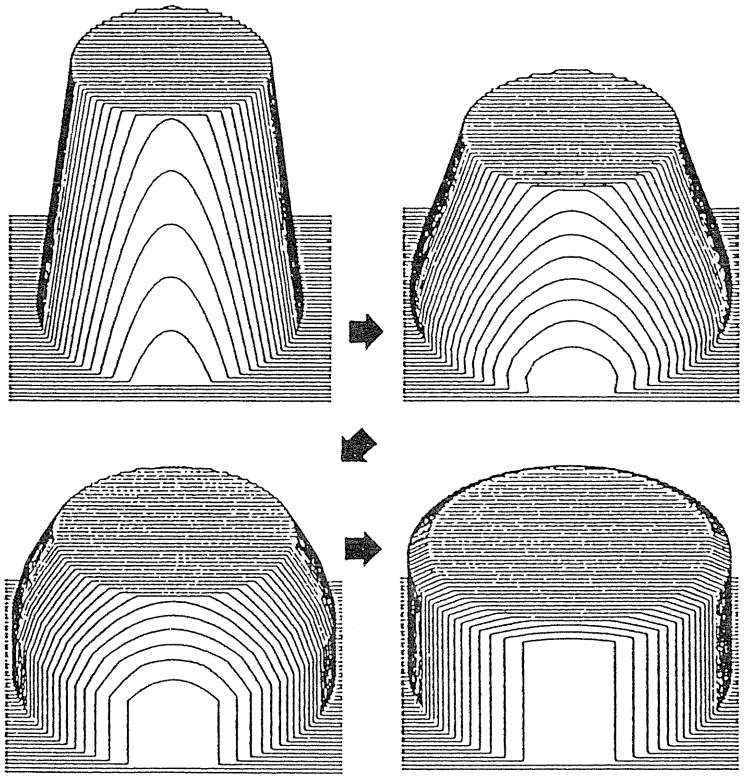

Fig. 37. Analytical result of deformation.

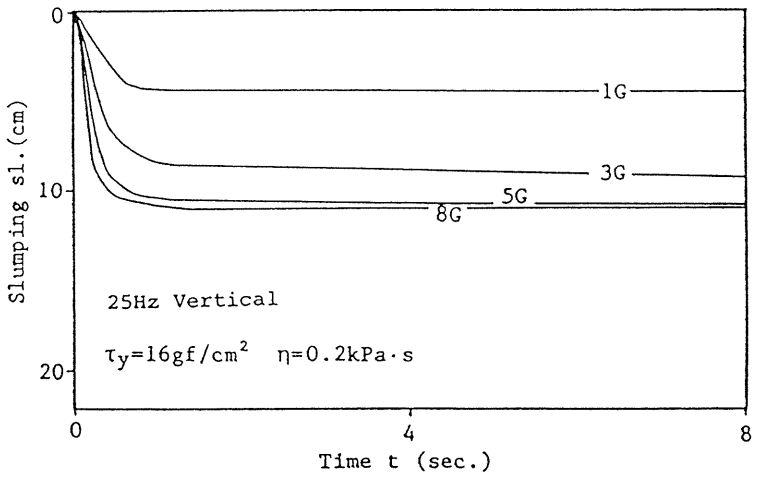

Fig. 38. Analytical result of effect of acceleration on slumping(sl.) – time(t) curves.

2. 8 Simulation of Flowing in a Small Model Form

Fig. 39 shows a small model form made of acrylic resin used in the experiment. First, half of the form is filled with fresh concrete, and when the central separator is pulled up, concrete starts to flow in the form. After the flow of fresh concrete under its own weight stops, the form is vibrated (60 Hz, 2g), and the relationship between the height of top surface of concrete and vibration time, i.e. the slumping − time curve, is measured until the concrete assumes a flat shape in the form.

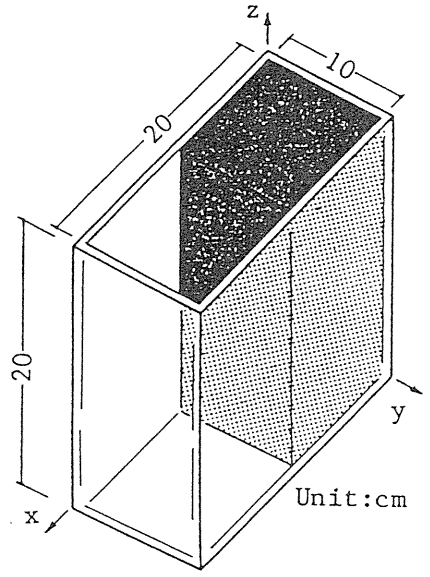

Fig. 39. Small modeled form.

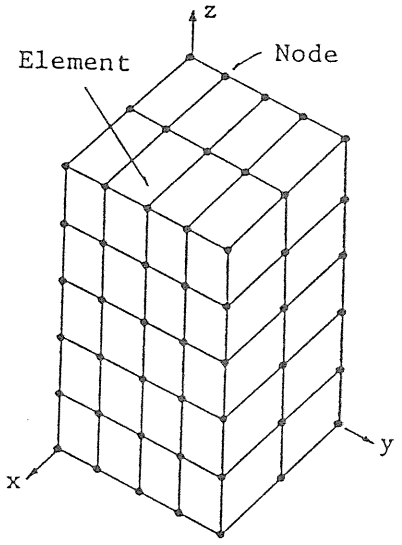

Fig. 40. Finite element idealization and coordinate.

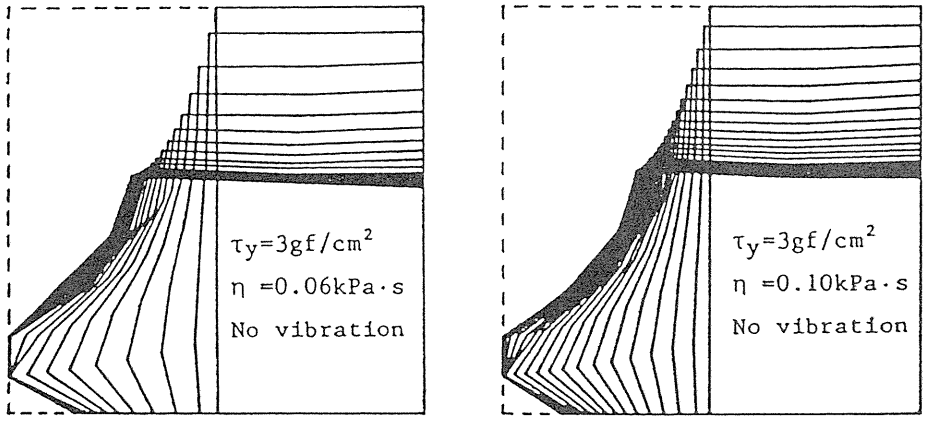

Fig. 41. Analytical result in the case of no vibration.

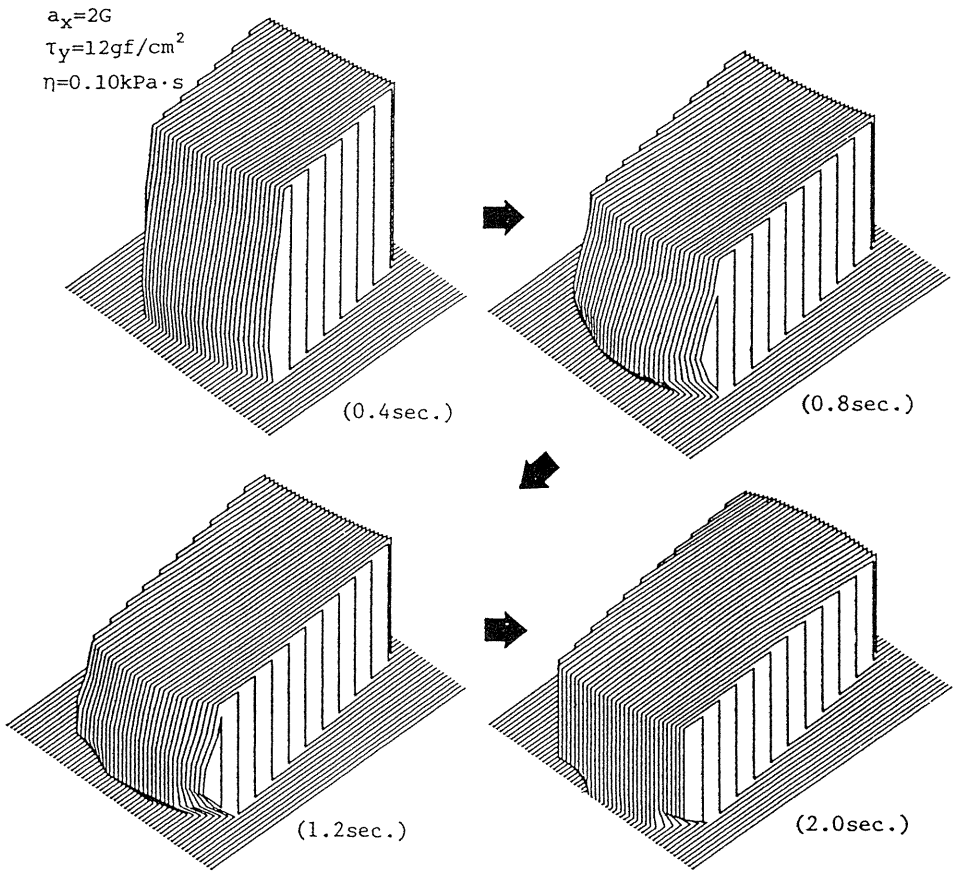

Fig. 42. Analytical result in the case of vibration.

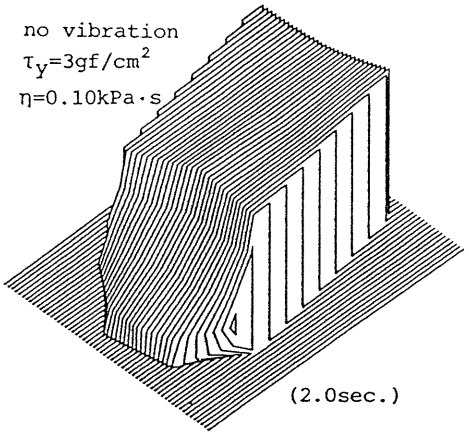

Fig. 43. Analytical result in the case of no vibration.

In the analysis, the shape and size of the form in the experiment were used as input data, and the finite element idealization shown in Fig. 40 was applied. Some examples of the analytical results are shown in Figs. 41—43. The analytical and experimental results of the flow of wet mixed mortar under no vibration are in good agreement, as shown in Figs. 43, 44 and Photo. 3. Fig. 45 compares measured and calculated slumping — time curves of fresh concrete subjected to vibration. The rheological constants used in the analysis as input data were estimated from the results of slump and flow tests. It is clear from this figure that while the shapes of measured and calculated slumping — time curves are similar, the calculated curves become flat earlier. The vibrating table used in the experiment gives rotating movement in the x-z plane, represented by a two-dimensional sinusoidal wave, but in this analysis a 1-directional rectangular wave used, as shown in Fig. 46, because of limited computer capacity.

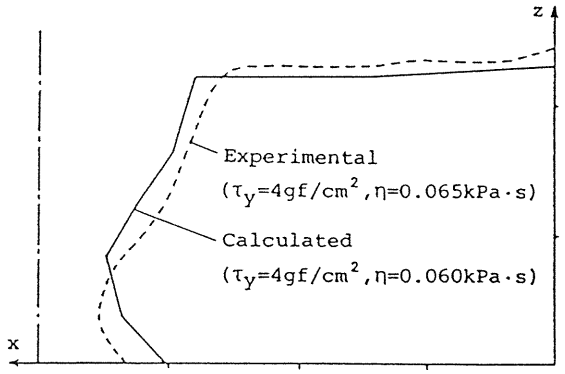

Fig. 44. Comparison between experimental and analytical results of shape at the surface of form.

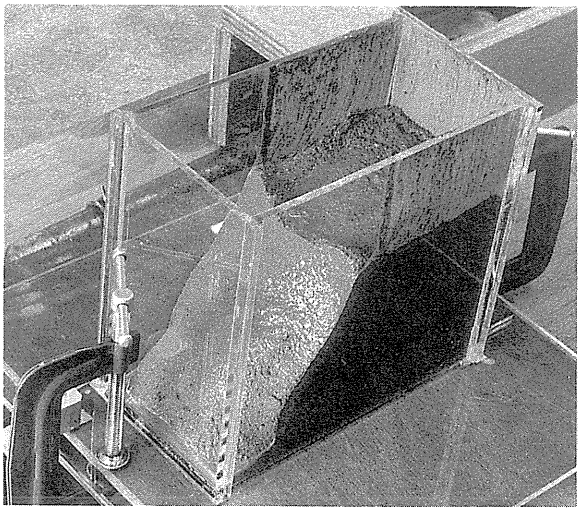

Photo. 3. Vibrating box test of mortar.

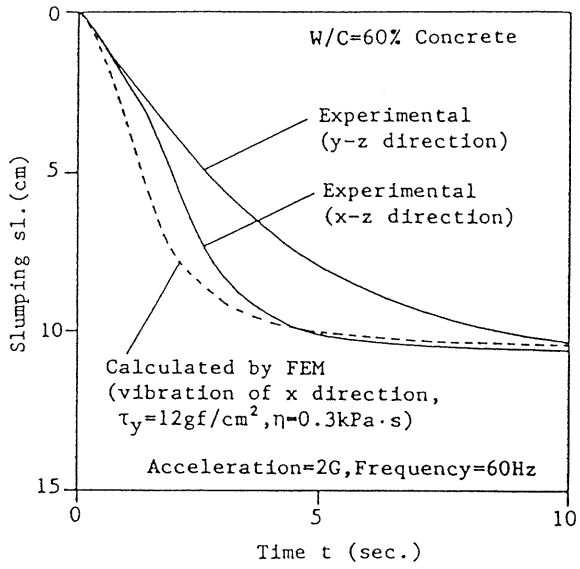

Fig. 45. Comparison between experimental and analytical results of slumping(sl.) – time(t) curves.

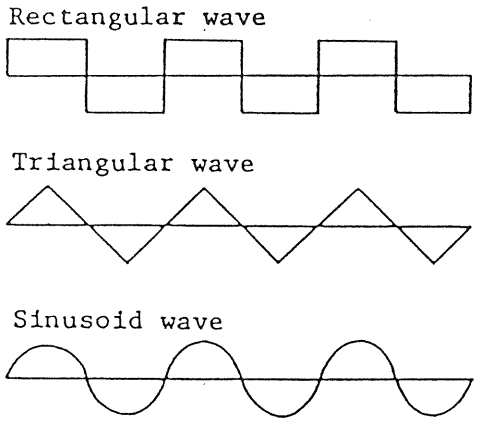

Fig. 46. Input waves of vibration.

The responses of the simplest structure, which consists of a single weight and element, by input acceleration of sinusoidal and rectangular waves are compared in Fig. 47, and the difference between the responses of two input waves in the Bingham model is larger than those in the Newtonian model, whose yield value is zero. The triangular wave was then used as input, and the analytical results shown in Fig. 48 were obtained, experimental and calculated curves agreeing well.

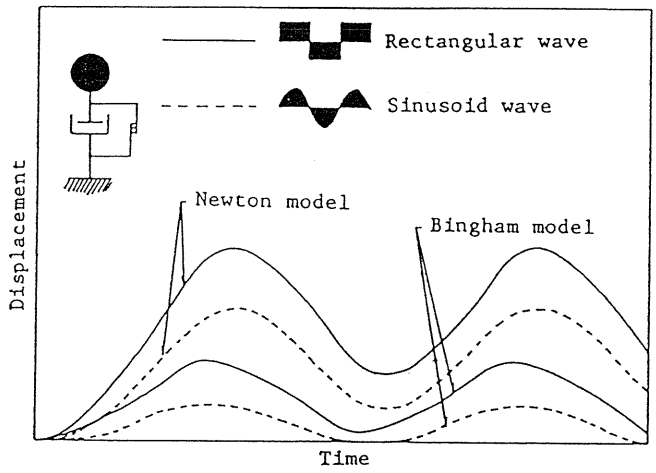

Fig. 47. Response of displacement in simple model.

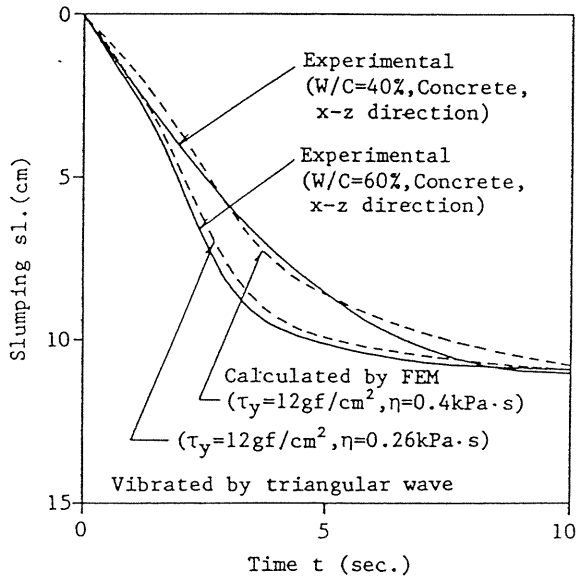

Fig. 48. Comparison between experimental and analytical results of slumping(sl.) – time(t) curves.

2. 9 *Simulation of VB Test*

The VB apparatus used in the experiment is shown in Fig. 49. In this experiment, normal concrete and under water concrete (1% dosage of segregation control agent by weight of cement) were used. The same vibrating table was used as for the small model form test described above.

An example of the analytical results is shown in Fig. 50; experimental and analytical

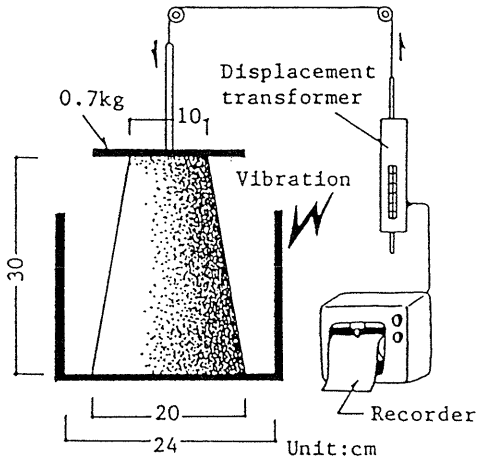

Fig. 49. VB test.

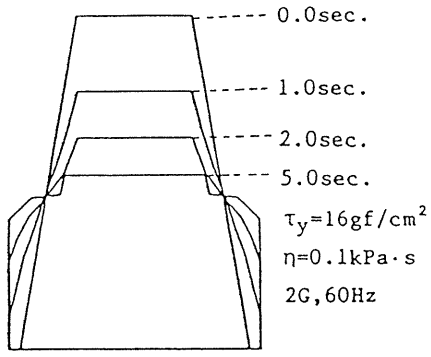

Fig. 50. Analytical result of deformation.

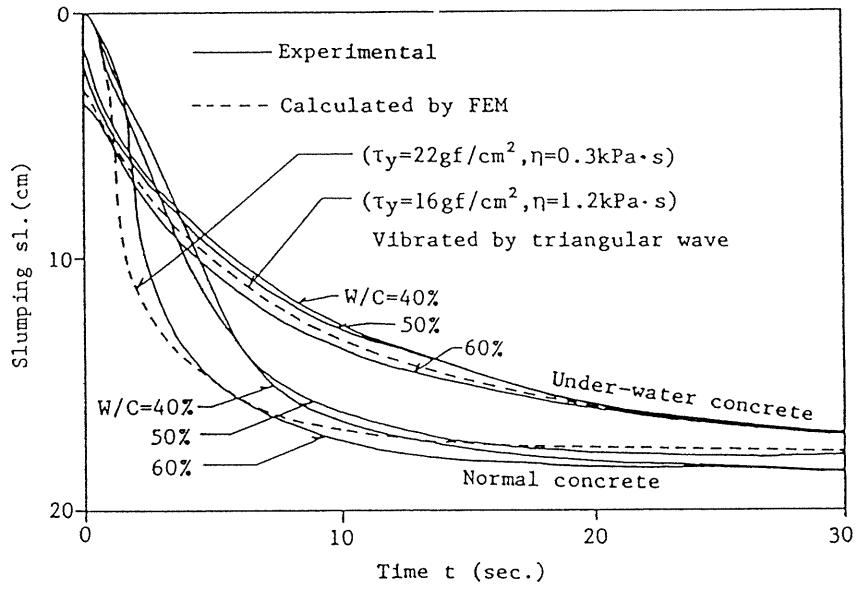

Fig. 51. Comparison between experimental and analytical results of slumping(sl.) – time(t) curves.

slumping – time curves are compared in Fig. 51. The analytical curves by triangular input wave can estimate the experimental result accurately, but the shape at the end of deformation is not flat in the analysis. This difference was also observed in simulating the vibrating consistency test mentioned above. For more accurate simulation it is necessary to investigate the segregation behavior of concrete from a rheological standpoint.

It is not easy to measure the rheological constants of comparatively dry mixed concrete exactly, because its properties cannot be expressed by a Bingham model due to the frictional and interlocking effect of aggregate. If such a technique is established, this analytical method should become more effective for the workability design of concreting works.

3. Viscoplastic Suspension Element Method

3. 1 Outline of Analysis

(1) Characteristics of Analysis

The characteristics of VFEM and VSEM (viscoplastic suspension element method) are shown in Table 7, and the process of calculation in VSEM is shown in Fig. 52. The flow of fresh concrete is resulted from the deformation of matrix between aggregates. To simulate the motion of stiff sphere particles in a viscoplastic body, cylindrical suspension elements with viscoplastic properties are constituted between a pair of particles when they are closer than a certain distance as shown in Fig. 53(a). Then the displacement of all particles are calculated based on the compressive and shear deformations of suspension elements as shown in Fig. 53(b). The deformation of fresh concrete is calculated

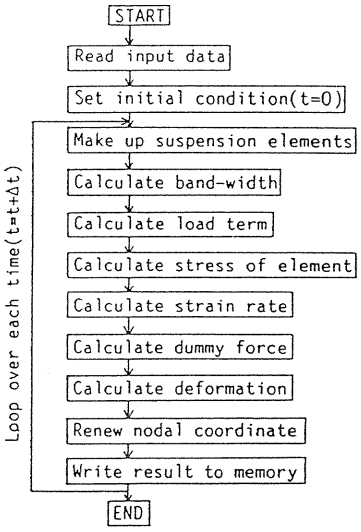

Fig. 52. Flow-chart of program for viscoplastic suspension element method (VSEM).

Table 7. Characteristics of VFEM and VSEM.

Suspension Element Method	Visco-plastic Finite Element Method
○ It is simple to dispose of restrictive condition. ○ Motion of node is flexible. (It is able to simulate complex behaviors of concrete such as collapse, separation, and mixing.) ○ Rheological constants of mortar can be used. (There are many experimental results on them.) ○ It is able to simulate the effects of aggregate and rheological properties of matrix. ▲ Large calculation time and memory are necessary.	○ Calculation time and memory used are relatively small. ○ Accuracy of calculation is good in case of homogeneous continuum model. ○ Rheological constants of concrete can be used. ▲ Segregation can not be analyzed. ▲ It is complex to dispose of restrictive condition.
Static Suspension Element Method	**Dymamic Suspension Element Method**
○ Stable solution can be obtained. ○ It is able to introduce the yield value in terms of stress state. ▲ It is necessary to calculate approximate force of inertia. ▲ It is necessary to dispose of free nodes.	○ It is unnecessary to calculate approximate force of inertia. ○ It is unnecessary to dispose of free nodes. ▲ When the yield value is high, the result of calculation becomes unstable.

at each 0.00001 sec.. The relative locations of particles change at each step, and suspension elements appear or disappear automatically. Thus complex flow behaviors of concrete related to aggregates can be analyzed by this method.

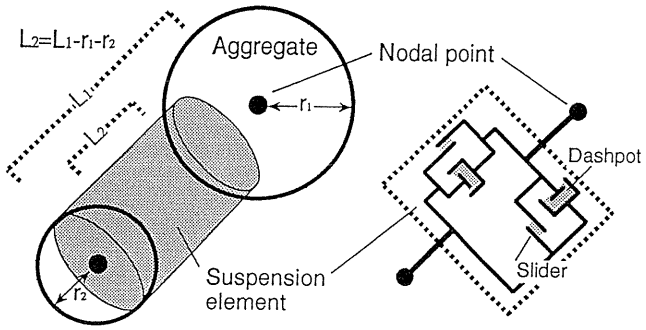

(a) Suspension element

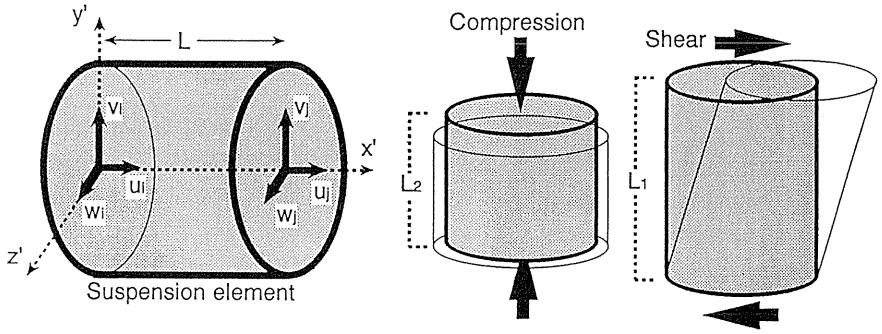

(b) Coordinate system and deformation of element

Fig. 53. Idealization of VSEM.

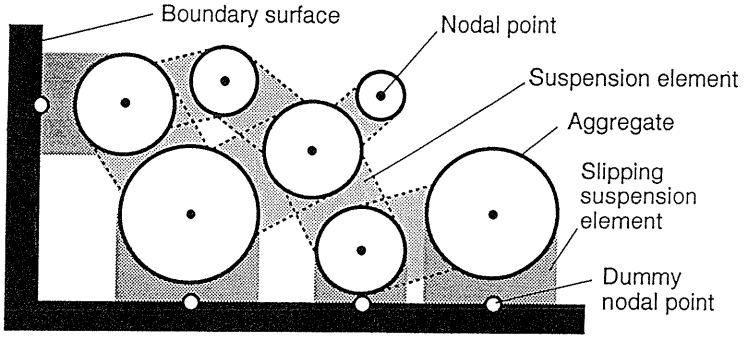

Fig. 54. Formation of suspension elements.

(2) Boundary Condition

For a particle near boundary surface, a slipping suspension element is constituted between the particle and boundary surface as shown in Fig. 54, which expresses the slipping resistance between fresh concrete and the surface of form or pipe, etc..

(3) Constitutive Law and Yield Function

In the present analysis, the constitutive law and yield condition of Bingham model which are expressed by yield value τ_y and plastic viscosity η are used to represent the rheological properties of fresh concrete.

(4) Coarse Aggregate and Mix Proportions

Coarse aggregates have various shapes and sizes in general, but, sphere particles with a certain diameter are used in this analytical method. When a coarse aggregate touches another one, the resisting elastic force will act between both particles. So the minimum length is assumed in this method, which will be a function of the shape of coarse aggregate. And the maximum length of suspension element should be a function of mix proportions i.e., the volume of matrix and aggregate. However it is very difficult to evaluate these functions, thus in this analysis, the constant values shown in Table 8 are used.

Table 8. Minimum and maximum lengths of suspension element.

$\ell_1=4\cdot r$, $\ell_2=2\cdot r$.
where,
r : radius of sphere,
ℓ_1: maximum length to constitute a suspension element,
ℓ_2: minimum length to estimate touch of two spheres.

3. 2 Examination of Analytical Method

A simple model test was carried out to examine the applicability of VSEM. The material used is consisted of 24 mm glass beads as coarse aggregates and 5% segregation control agent diluted with water as matrix. An acrylic model form as shown in Fig. 55 was used, and the flow behavior was recorded by a high speed VTR system. The material is cast into the left side of the form as shown in Photo. 4(a), and starts to flow toward the right side by the self-weight after pulling up the separator. Experimental results are shown in Photo. 4(b) and Photo. 4(c), and analytical ones by VSEM are shown in Fig. 56. According to these figures, it can be said that this analytical method has enough accuracy to estimate the flow behavior of fresh

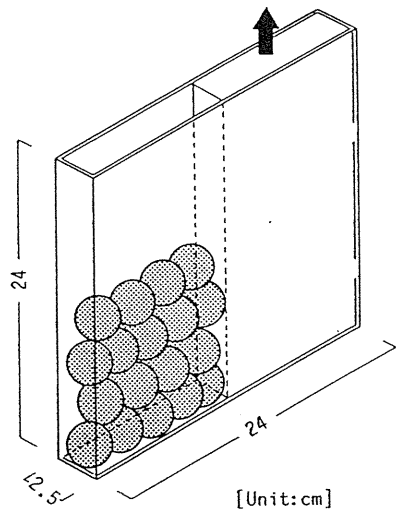

Fig. 55. Two-dimensional modeled form.

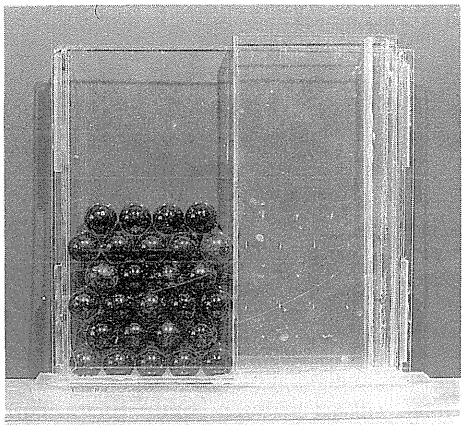

(a) 0sec.

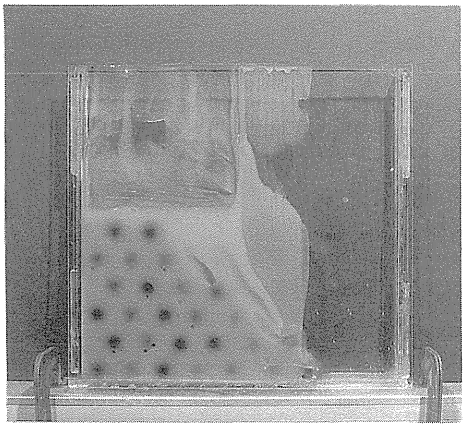

(b) 8sec.

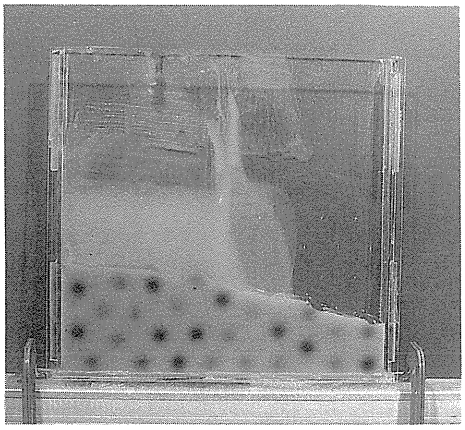

(c) 20sec.

Photo. 4. Experimental result of flow behavior in two-dimensional form.

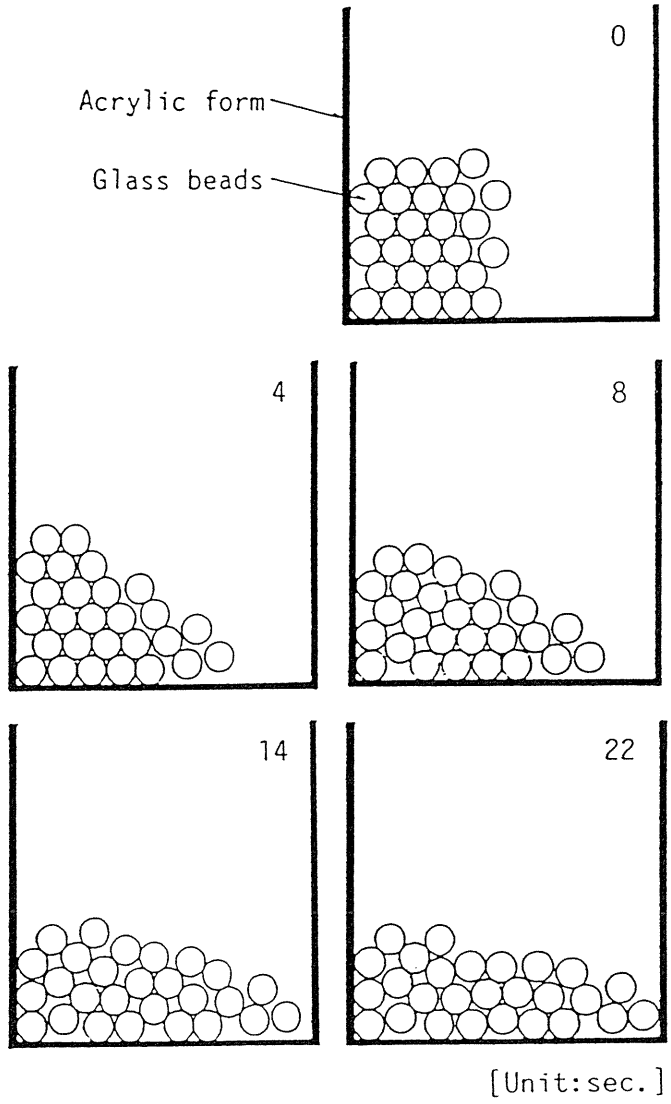

Fig. 56. Analytical result of flow behavior in two-dimensional form.

concrete. A little difference between experimental and analytical results may be resulted from the following causes: the variety of size of glass beads used, a little vibration caused when the separator is pulled up, and some assumptions used in the analytical method, and so on.

An analytical result of the flow behavior in three-dimensional model form is shown in Fig. 57. The suspension element method can be easily applied to three-dimensional problems.

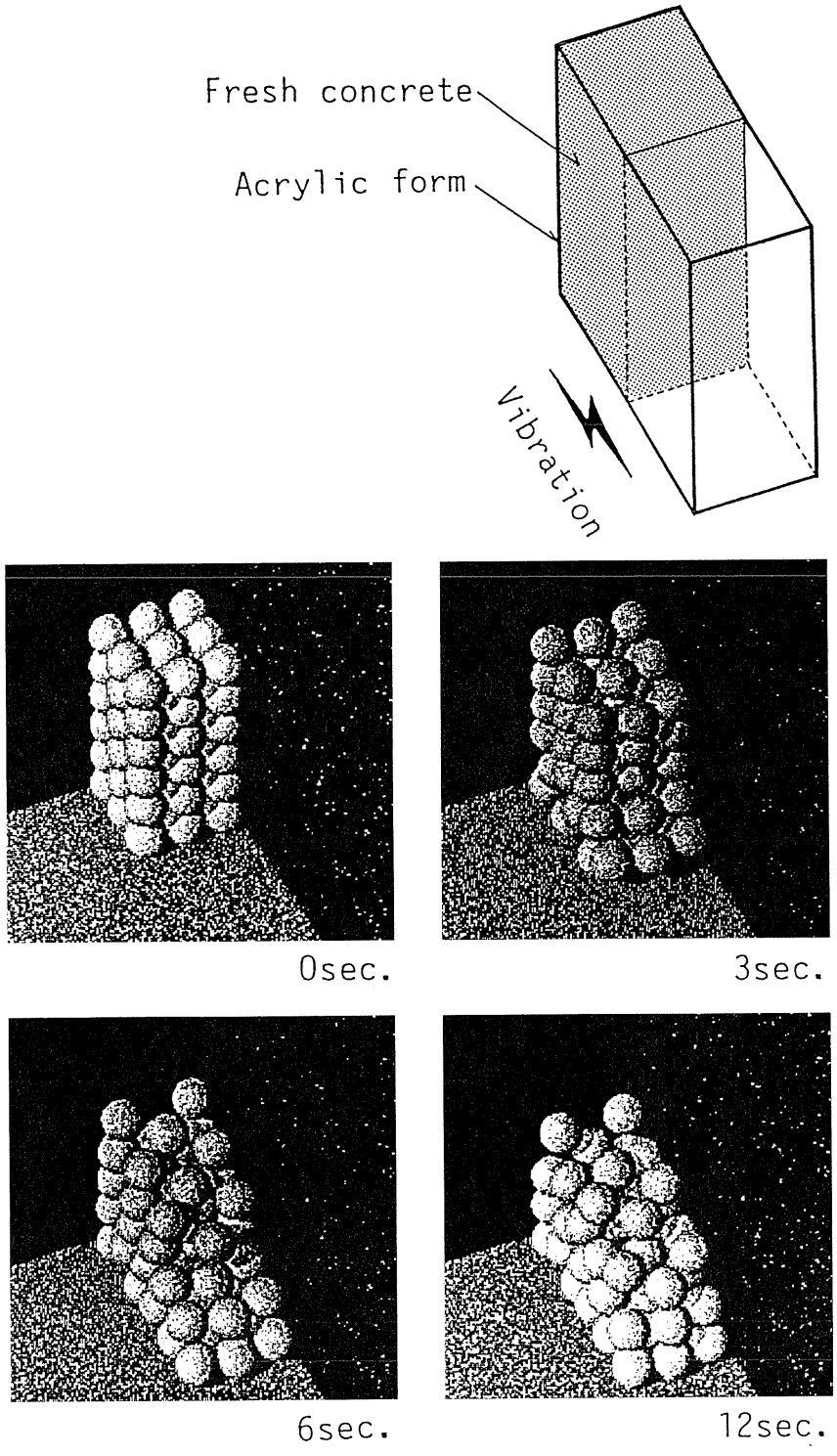

Fig. 57. Analytical result of flow behavior in three-dimensional form.

3. 3 Simulation of Slump Test

A two-dimensional slump test was simulated as a simple example. The touch of concrete to the slump cone at lifting is not considered. Fig. 58 and Fig. 59 show the analytical results.

The shape of top surface and the deformation behavior affected by the rubbing of bottom surface are similar to the analytical results obtained by the VFEM mentioned above. They are also similar to the experimental results by the actual slump test. Aggregates fall down unsymmetrically because the initial aggregate location is not necessary symmetrical.

The rheological constants shown in Fig. 58 and Fig. 59 correspond to those of mortar matrix in the concrete. The rheological constants in Fig. 59 are higher than those in Fig. 58, and these figures correspond to wet and dry mixed concrete with the same volume of coarse aggregate, respectively.

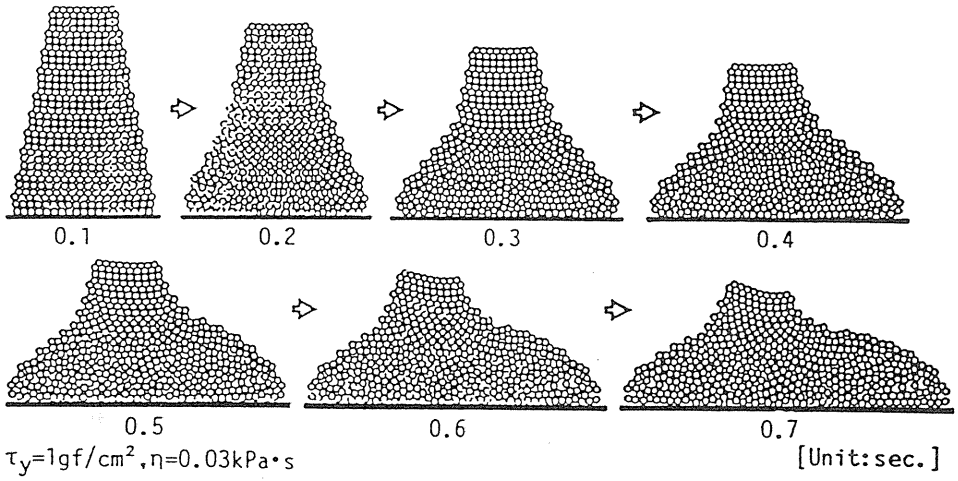

Fig. 58. Analytical result of two-dimensional slump test (Wet mixed concrete).

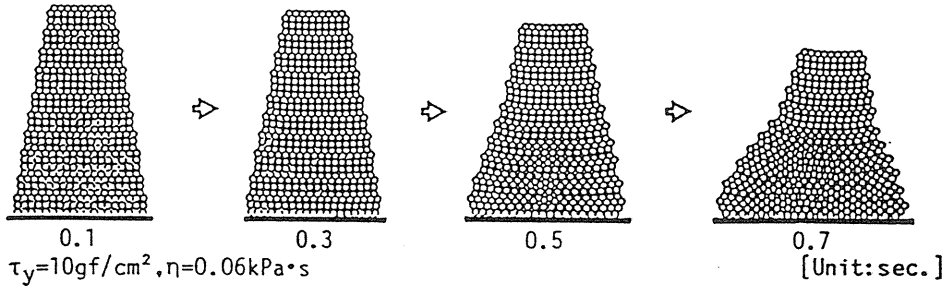

Fig. 59. Analytical result of two-dimensional slump test (Dry mixed concrete).

3. 4 Simulation of L-type Flow Test

The apparatus of L-type flow test developed to estimate the consistency of high and ultra-high strength concrete is shown in Fig. 60. Concrete flows from the exit at the lower

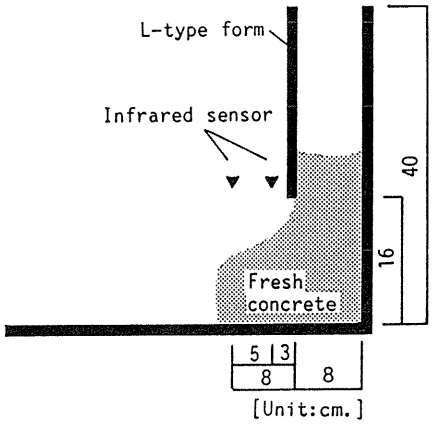

Fig. 60. L-type flow test.

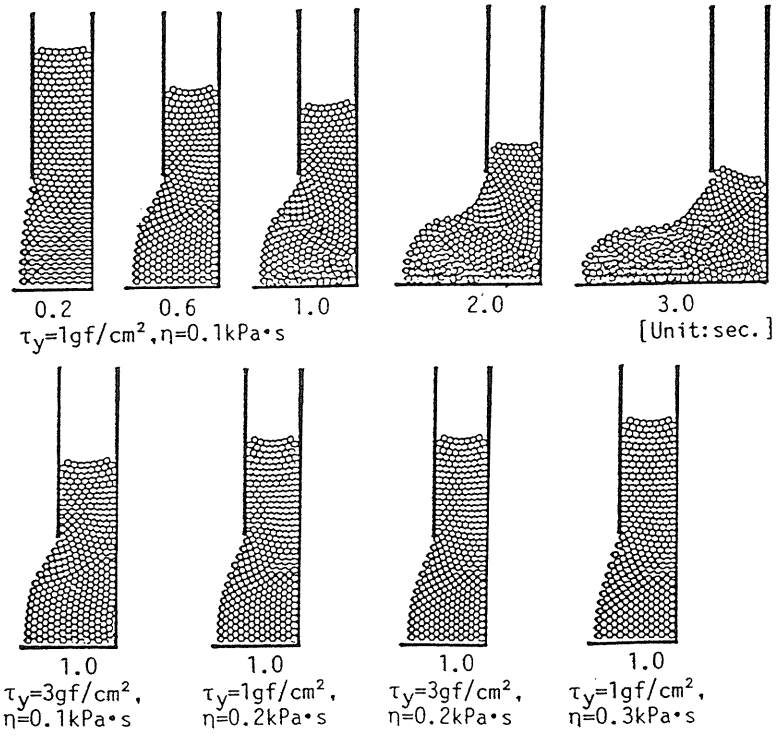

Fig. 61. Analytical result of L-type flow test.

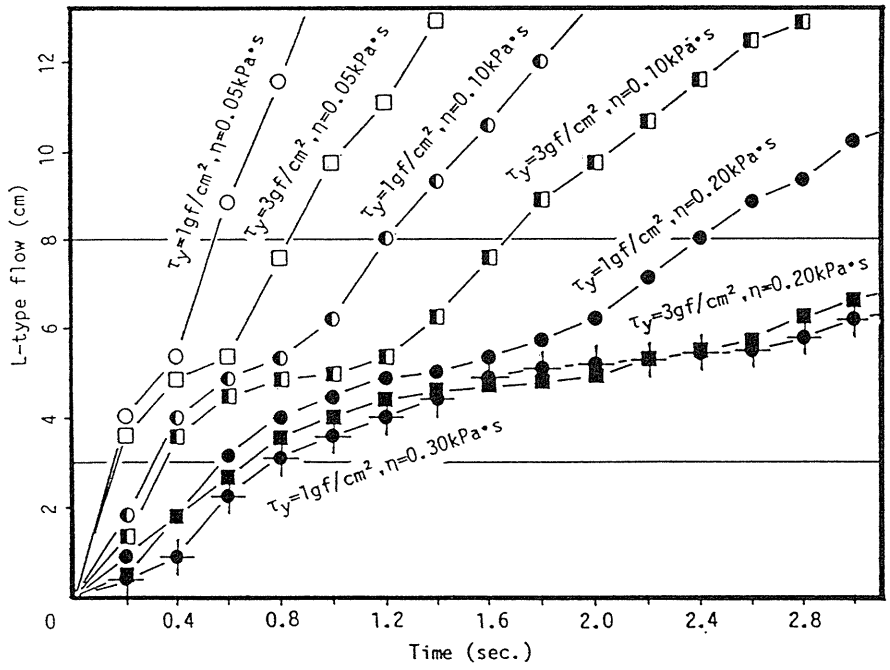

Fig. 62. Analytical result of relationship between L-type flow and time.

portion of form, and the slump and flow values (L-type slump value and L-type flow value, respectively) are measured. These values are used for expressing the consistency of fresh concrete.

The simulation of L-type flow test was carried out as a two-dimensional problem. Analytical results are shown in Fig. 61 and the flowing – time relation is shown in Fig. 62. As shown in these figures, the flow behavior is affected by the yield value and the plastic viscosity.

A pair of infrared sensors were set on the apparatus (one was set at 3 cm and the other at 8 cm from the exit). They are turned on and off respectively when fresh concrete reaches to the locations, and the velocity of flow (L-type flow velocity, Lfv) was measured. The relationship between L-type flow velocity and plastic viscosity obtained by the analysis is shown in Fig. 63. It may be possible to estimate the yield value and the plastic viscosity of fresh concrete by the slump value and the initial velocity of L-type flow.

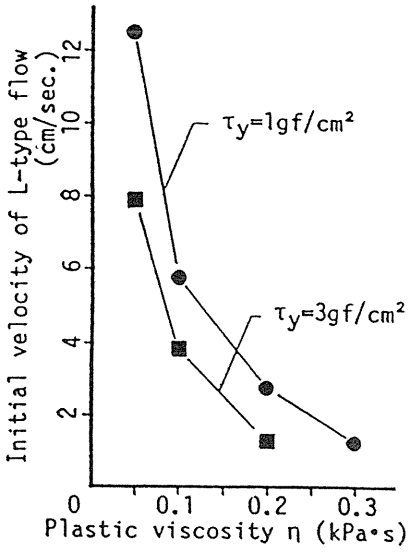

Fig. 63. Relationship between L-type flow velocity and plastic viscosity.

3. 5 *Simulation of Vibrating Box Test*

It is necessary to consider the effects of reinforcement and vibration for examining the compactability of fresh concrete in a form. Especially, the flowability of fresh concrete in narrow space between reinforcements and the cohesive force between matrix and coarse aggregate are important. The space between reinforcements is related to the size and amount of coarse aggregate, and the cohesive force is affected by vibration. It is difficult to estimate the effects of these factors by an analytical method using an uniform continuous model in VFEM. The VSEM using the two phase model can be applied to analyze these behaviors directly.

The authors have carried out a box test on a vibration table and obtained the test results related to the behavior of fresh concrete under vibration[14]. Fig. 64 shows the shape and size of the apparatus used, and Fig. 65 shows the analytical results of the box test. A black triangle mark shown in Fig. 65 indicates the height of fresh concrete obtained by the experiment. The rheological constants, frequency and acceleration of vibration obtained by the experiment were used in the analysis.

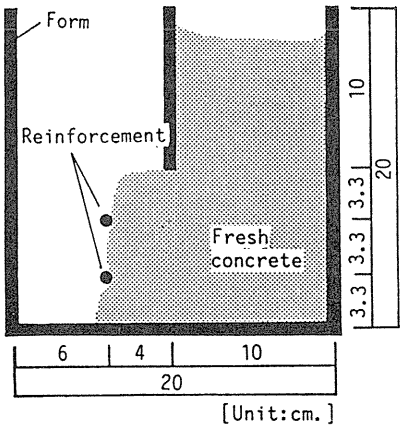

Fig. 64. Vibrating box test.

The flow of fresh concrete stopped at the location of reinforcement under no vibration (this behavior is not shown in the figure), but as shown in Fig. 65, fresh concrete becomes very flowable subjected to vibration. The shape of concrete flowing out from the exit is similar to that observed by the experiment. According to the analytical result in Fig. 65, the right lower part of fresh concrete hardly deforms, and the upper part covering the lower part flows out the left side.

When the reinforcing bars are arranged as shown in Fig. 65(b), coarse aggregates flow to the left side avoiding them, and concrete does not flow so easily as in the case of no reinforcement. The VSEM appears to explain the experimental results fairly well, though the analysis is two-dimensional.

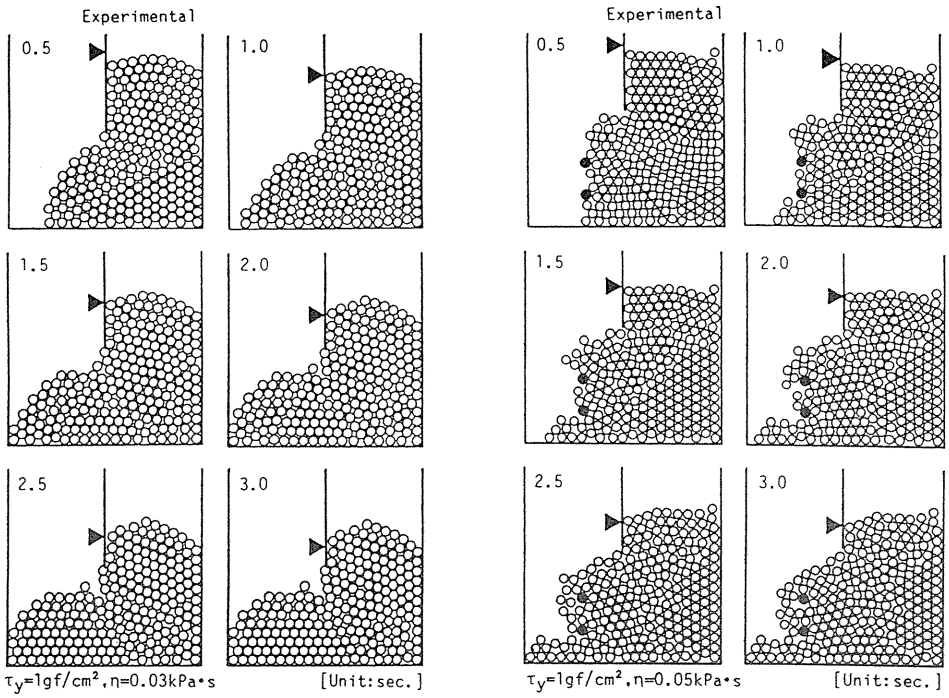

(a) No reinforcement (b) With reinforcement

Fig. 65. Analytical result of flow behavior in vibrating box test.

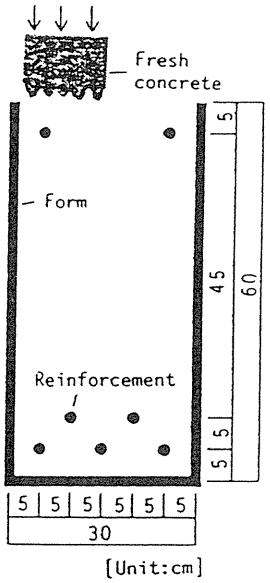

Fig. 66. Size of RC beam.

3. 6 Simulation of Casting into Formwork of RC Beam

As an example of a more practical concreting work, a simulation of casting to a form of RC beam was carried out. The size of section and analytical idealization are shown in Fig. 66, and the analytical results are shown in Fig. 67. As shown in Fig. 67(a) which indicates the result for wet mixed concrete, complex behaviors such as separating and gathering of coarse aggregates can be simulated. As shown in Fig. 67(b) which indicates the result for dry mixed concrete, the casting velocity becomes slower than that for wet mixed one.

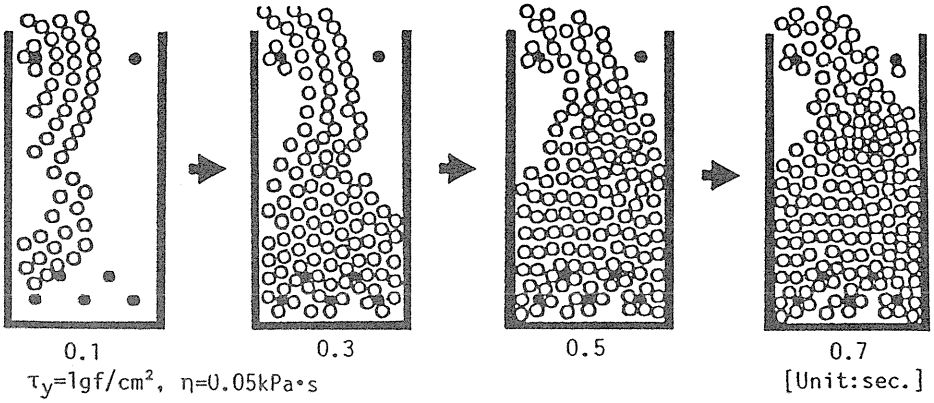

(a) Wet mixed concrete

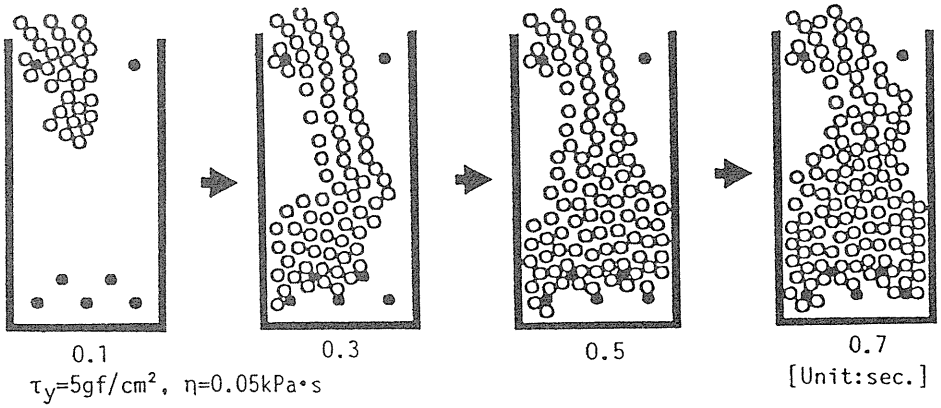

(b) Dry mixed concrete

Fig. 67. Analytical result of casting to RC beam.

3. 7 Simulation of Casting into Formwork of RC Wall

The size of section of RC wall used for the analysis and the analytical results are shown in Fig. 68 and Fig. 69, respectively. The reinforcements are located parallel to the form at the

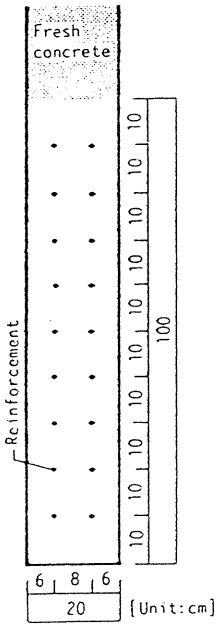

Fig. 68. Size of RC wall.

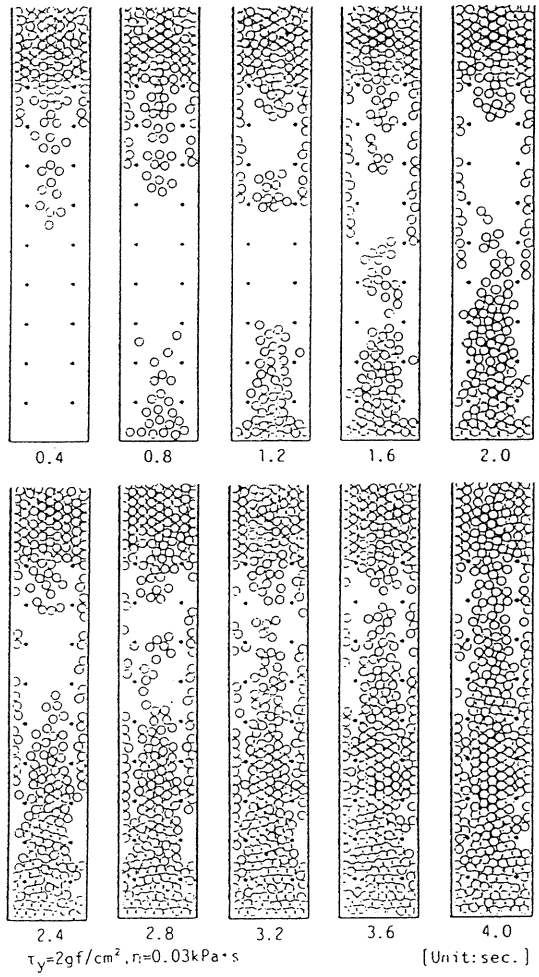

Fig. 69. Analytical result of casting to RC wall.

spacing of 10 cm. It is supposed that there is a large amount of concrete in the portion over the height of 100 cm as in the casting by bucket, and nodal force corresponding to the weight of fresh concrete existing in the upper portion over 100 cm acts on each coarse aggregate.

The flow of fresh concrete is arrested by the highest reinforcement, concrete flows to the center portion of the section, then fresh concrete near the form falls down, as shown in Fig. 69. Fresh concrete cast in the center portion of the form hardly flows to the portion of the cover of reinforcement. In this analysis, a constant size of coarse aggregate is used but it may be possible by using various sizes of coarse aggregate to estimate more accurately the flow behavior of fresh concrete considering the bearing effect by small size of aggregate and the compactability of fresh concrete in narrow space such as the cover portion of reinforcement.

3. 8 Simulation of Pumpability in Tapered Pipe

(1) Outline of Analysis

The simulation is carried out by using simple models of two-dimensional tapered pipe. Two different series of examples are prepared in this analysis, i.e., H and V series in which pipes are set horizontally and vertically respectively. The shape and size of modeled tapered pipes used are shown in Fig. 70 and Table 9. Aggregates in fresh concrete flowing in pipe appear near the entrance of pipe (section S), and disappear near the exit (section E). A certain pressure is loaded to aggregates before the section A in the axial direction of pipe. Input data of pumping pressure, rheological properties of matrix and slipping resistance are shown in Table 10. The values of slipping resistance were obtained by the experiment mentioned above. The diameter of particles (aggregates) is 10 mm in this simulation.

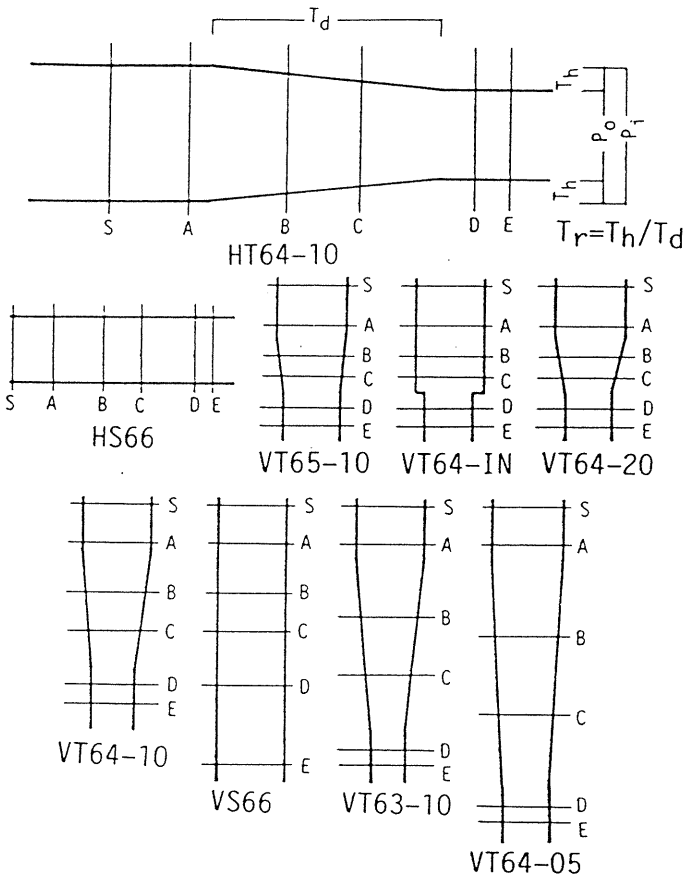

Fig. 70. Form of modeled pipe and section for simulation.

Table 9. Shape and size of modeled pipe.

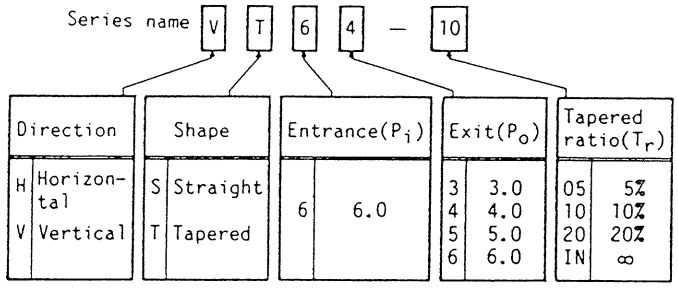

Series	S∿A	A∿B	B∿C	C∿D	D∿E
HS66	3.5	4.3	3.3	4.8	1.5
VS66	3.5	4.3	3.3	4.8	6.5
HT64-10	3.5	4.3	3.3	4.8	1.5
VT64-IN	3.5	2.7	1.7	3.2	1.5
VT64-10	3.5	4.3	3.3	4.8	1.5
VT63-10	3.5	6.0	5.0	6.5	1.5
VT65-10	3.5	2.7	1.7	3.2	1.5
VT64-05	3.5	7.7	6.7	8.2	1.5
VT64-20	3.5	2.7	1.7	3.5	1.5

Unit:cm.

Table 10. Input data of fresh concrete.

A_g(mm)	η(kPa•s)	τ_y(gf/cm^2)
10	0.05∿0.10	1.0∿10.0

S_1	S_2	S_3	S_4
0.00∿0.04	0.0∿0.7	0.1∿0.3	0.7∿2.5

[Notes]
A_g:Size of aggregate, η:Plastic viscosity, τ_y:Yield value, S_1∿S_4: Parameters in the following equation ; $\sigma_h=S_1\beta\sigma_n+S_2\beta+S_3\sigma_n+S_4$, σ_h:Slipping resistance stress (gf/cm^2), β: Slipping velocity (cm/sec), σ_n:Normal stress (gf/cm^2).

(2) Horizontal Pipe

Several analytical results obtained by H series are shown in Fig. 71. In this figure, some aggregates are marked to clarify the motion of aggregates, and the plug flow can be observed.

As shown in the analytical results, the flow behavior is considerably complicated by slipping resistance between concrete and wall of pipe, especially in case of horizontal pipes. In this paper, to clarify the effects of rheological properties of fresh concrete and shape of pipes on the flow behavior, the results obtained by V series (vertical pipes) are discussed in the following, in which the slipping resistance has less influence on the flow behavior of fresh concrete than that in H series.

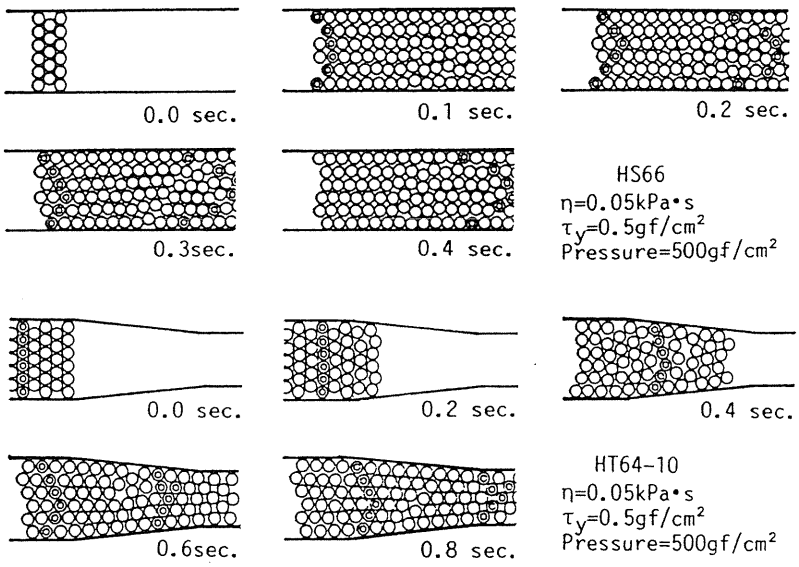

Fig. 71. Analytical results of flow behavior in modeled pipe (H series).

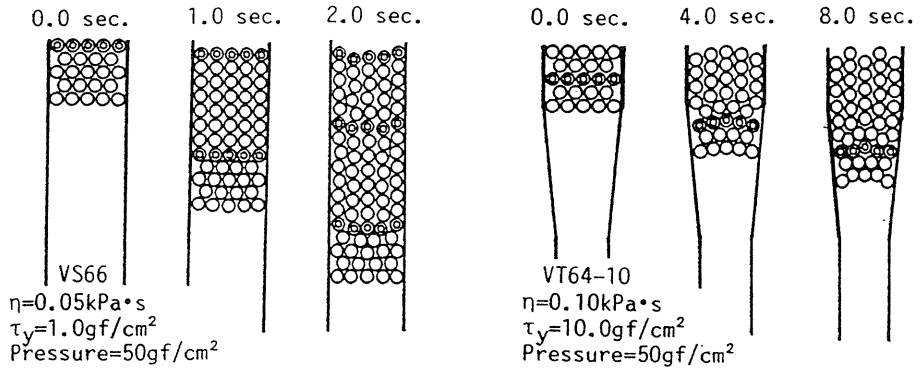

Fig. 72. Analytical results of flow behavior in modeled pipe (V series).

(3) Vertical Pipe

Some examples of analytical results obtained by V series are shown in Fig. 72. The flow velocity at each section of pipes is calculated from the analytical results, and used in the following discussion.

Fig. 73 shows an example of analytical results indicating the relationship between flow velocity and position x of aggregates in pipe. As shown in this figure, the flow velocity is almost constant except for the portion near the entrance, and the plug flow can be observed in every portion.

The relationship between average velocity in each section and time t is shown in Fig. 74. The sections (A-D) in Fig. 74 are as shown in Fig. 70 mentioned above. It is clear in this figure that the flow velocity in each section decreases with time, and tends to become constant gradually.

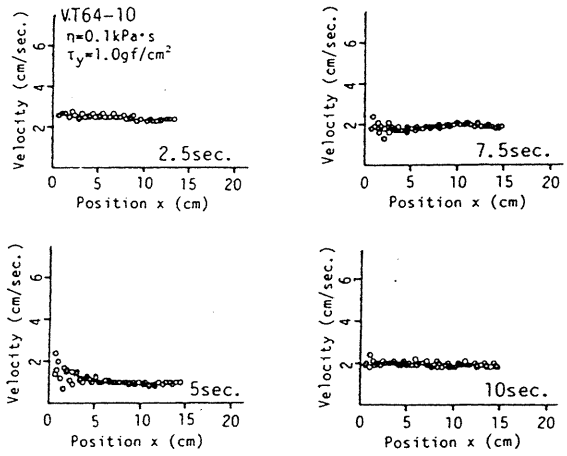

Fig. 73. Relationship between flow velocity and position (x) of aggregates in pipe.

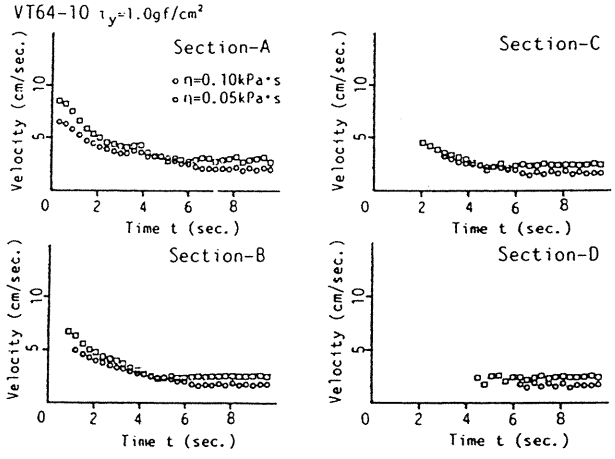

Fig. 74. Relationship between flow velocity and time (t).

In Fig. 75, the flow velocities in a straight pipe (VS66) and a tapered pipe (VT64-10) are compared. The flow velocities in the straight pipe are larger than those in the tapered pipe, and decrease with the increase of the distance from entrance because of the friction between concrete and inside wall of pipe. The flow velocities in the tapered pipe, however hardly change in the section B through D.

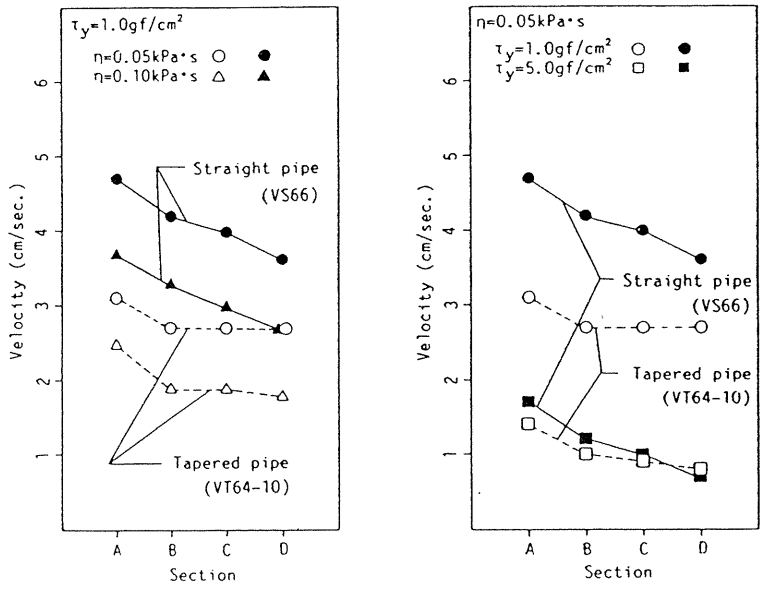

Fig. 75. Comparison of flow velocities in straight pipe and tapered pipe.

The effects of yield value and plastic viscosity of fresh concrete flowing in tapered pipes on the flow velocity are shown in Fig. 76 and Fig. 77, respectively. It is shown in these figures that the flow velocities decrease, or the interlocking of fresh concrete occurs with increasing yield value and plastic viscosity.

As shown in Fig. 76(a) and Fig. 77(a), the flow velocities decrease with the decrease of diameter of exit Po for the same tapered ratio Tr, because the resistance against flow becomes large. On the other hand, as in Fig. 76(b) and Fig. 77(b), the flow velocity in the section D (non-tapered section) increases with increasing tapered ratio Tr when the yield value is small. When the yield value becomes large, however, the flow velocity decreases with increasing tapered ratio, as shown in Fig. 76(b). That is to say, there is the most rational tapered ratio, and it is affected by rheological constants of fresh concrete.

In Fig. 78, the flow velocity in a tapered pipe is compared with that in the pipe which is jointed two pipes with different diameters. No blocking is observed at the jointed portion in this analysis, but the flow velocities in the jointed pipe are considerably smaller than those in the tapered pipe. As shown in Fig. 70 and Fig. 71 mentioned above or in a previous experimental study[15], the aggregates in concrete pumped in pipe tend to accumulate at tapered portions. In this analysis, the complete formation of blocking can not be expressed, because the frictional resistance is not introduced at the surface of aggregates touching each other.

The factors affecting the mechanism of blocking would be able to clarify analytically, provided that the parameters related to the friction between aggregates are known.

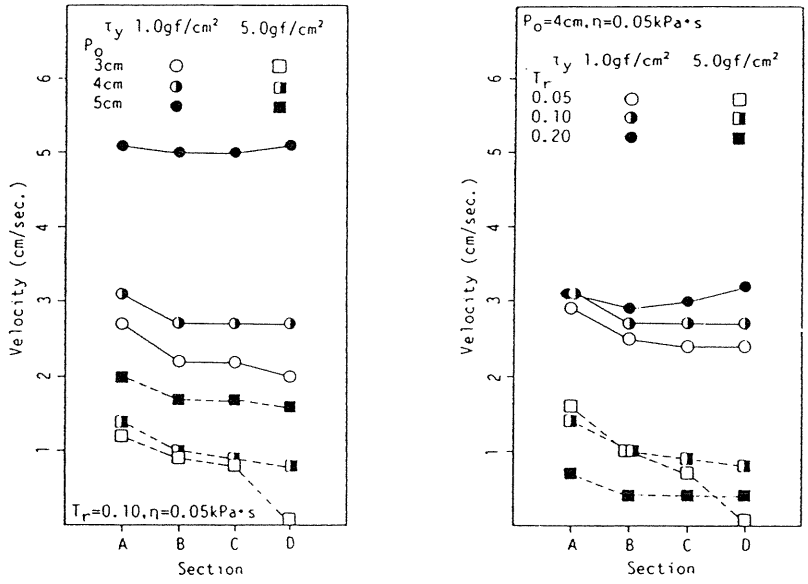

Fig. 76. Effect of yield value on flow velocity.

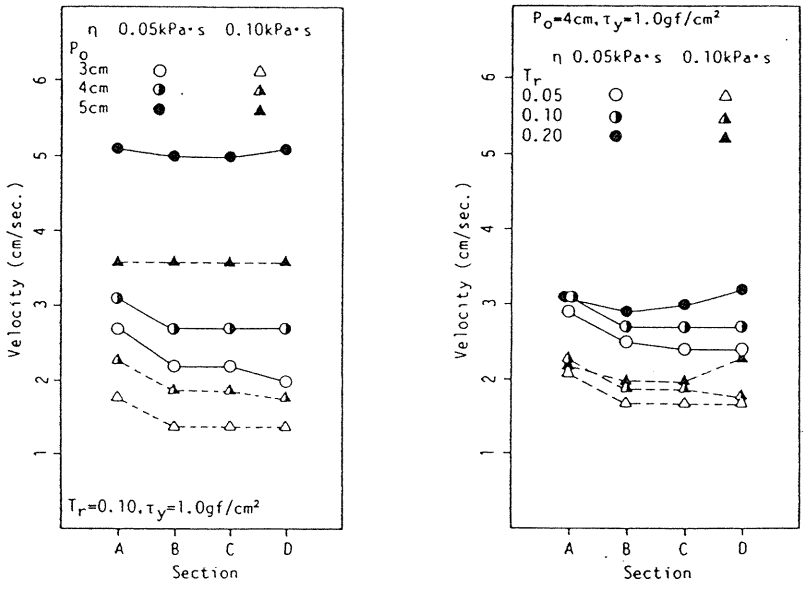

Fig. 77. Effect of plastic viscosity on flow velocity.

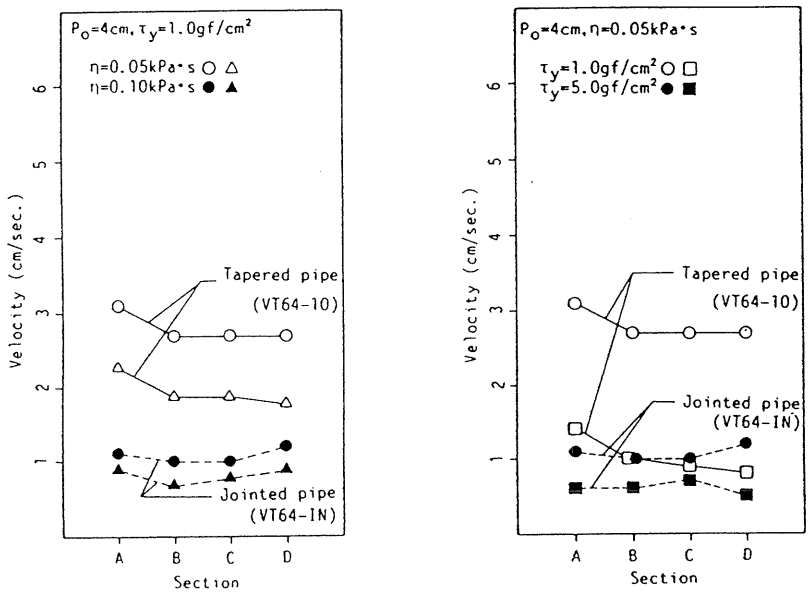

Fig. 78. Comparison of flow velocities in jointed pipe and tapered pipe.

4. Viscoplastic Divided Space Element Method

4. 1 Outline of Analysis

(1) Characteristics of Analysis

The characteristics of viscoplastic divided space element method (VDEM) are shown and compared with those of VFEM in Table 11.

Table 11. Characteristics of VDEM and VSEM

Items	Viscoplastic divided space element method - VDEM -	Viscoplastic finite element method - VFEM -
Input parameters	*Rheological constants of fresh concrete.	*Rheological constants of fresh concrete.
Analytical method	*Divide all space into elements and cells, and calculate whether fresh concrete exists in each cell or not.	*Divide fresh concrete into elements, and calculate deformation of elements.
Description of flow	*Displacement of markers.	*Displacement of nodal points.
Characteristics	*Large deformation, separating and gathering are easily analized. *This method is applicable to macro problem. *Accuracy of solution depends on size of cell. *Boundary condition is simple.	*Applicable subjects are limited for restraint of element construction. *This method is applicable to micro problem. *Accurate solution can be obtained if deformation is small. *Boundary condition is complicated.

In this simulation method, the space where concrete will be cast in form is divided into finite elements before calculation. Two-dimensional quadratic elements with 8 nodal points are used as space divided elements in the analysis. Each space element has nine — 3 by 3 — integral areas, and those small areas are called "cell" herein. Every cell has each attribute of the material filled there. For example, in the present analysis, two types of attributes are prepared corresponding to existence or none of fresh concrete in the portion, and more numbers of attributes can be used for more complex simulation.

The process of calculation in VDEM is shown in Fig. 79. In the calculation of VFEM, the coordinates of nodal points are changed with time step according to the deformation rate of each element, but in that of VDEM, the markers in elements displace instead of nodal points. The deformation of fresh concrete is expressed by the displacement of the markers in VDEM, and it is most different from the simulation by VFEM where the deformation is expressed by the displacement of nodal points. The coordinates of markers are calculated by the displacement rate of nodal points obtained by calculation at each time step. The process of calculation is similar to the MAC method used in general hydrodynamics simulation for air and liquids.

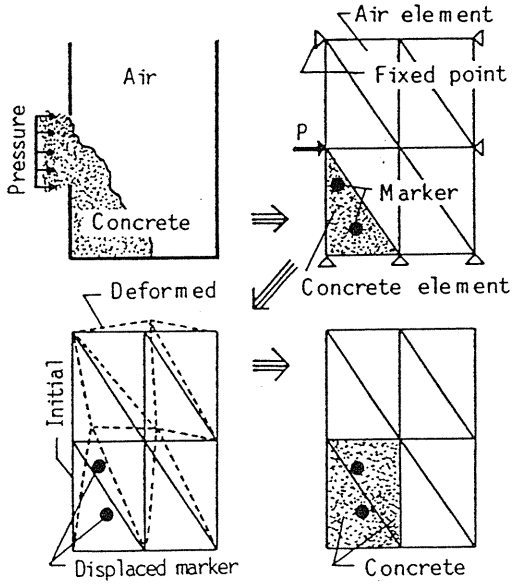

Fig. 79. Process of calculation in viscoplastic divided space element method (VDEM).

(2) Marker and Cell

The attribute of cell is switched according to the kind of material, air or concrete in it, and varies with each time step. When a marker comes into a certain cell, this cell is assumed to be full with fresh concrete, that is, the cell has the attribute of concrete. If a material consists of three or more components, it is necessary to give three or more attributes to the markers, and to consider a switching rule of cell attribute according to the attributes of markers.

(3) Method of Calculation

The viscoplastic calculation technique in VDEM is the same with that in VFEM, whose applicability has been examined by many simulations and experimental results mentioned above. Force such as pressure is input as the equivalent nodal force, and the selfweight of material is calculated according to the attribute of cell at each step of time to obtain the equivalent nodal force. In this analysis, all nodal points on the surface of form wall are treated as fixed points. For more accurate analysis or saving computed memory, slipping elements can be used which are applied in VFEM analysis.

In the present analysis, the constitutive law and yield condition for the Bingham model are used to express the rheological properties of fresh concrete. The computer program has been developed from that for VFEM.

The flow chart of VDEM is shown in Fig. 80. It is assumed that the yield value and the plastic viscosity of the cell with attribute of air is zero and 0.01 times of that of fresh concrete, respectively.

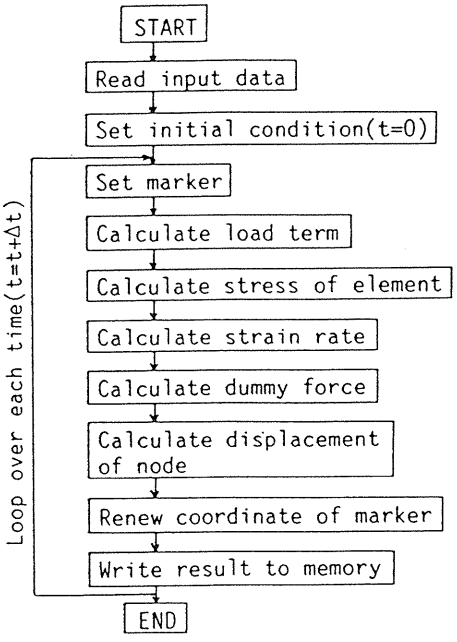

Fig. 80. Flow-chart of program for VDEM.

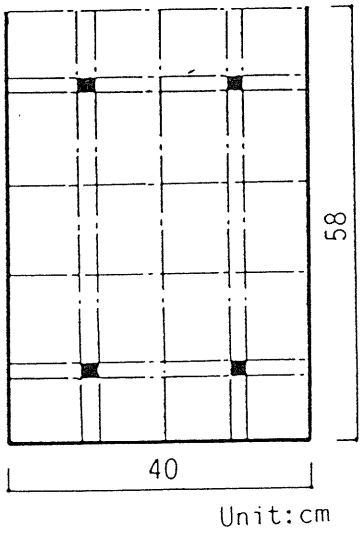

Fig. 81. Section and idealization for simulation.

4. 2 Simulation of Casting into RC Beam

Some analytical results of the flow behavior of fresh concrete cast into a section of RC beam are shown. The shape of the section and the idealization to space divided elements are illustrated in Fig. 81. The analytical results are shown in Fig. 82 and Fig. 83 with the input values of rheological constants for wet mixed and dry mixed concretes, respectively. As shown in these figures, the complex behaviors of fresh concrete, such as separating or gathering, can be simulated by the analysis because of the flexibility of this analytical model, in

which the deformation of fresh concrete is expressed by the displacement of markers, not of nodal points. Furthermore, the boundary condition is easily introduced in this analysis to consider the shape of section and the arrangement of reinforcements, because all elements never deform and all fixed nodal points never displace through calculation.

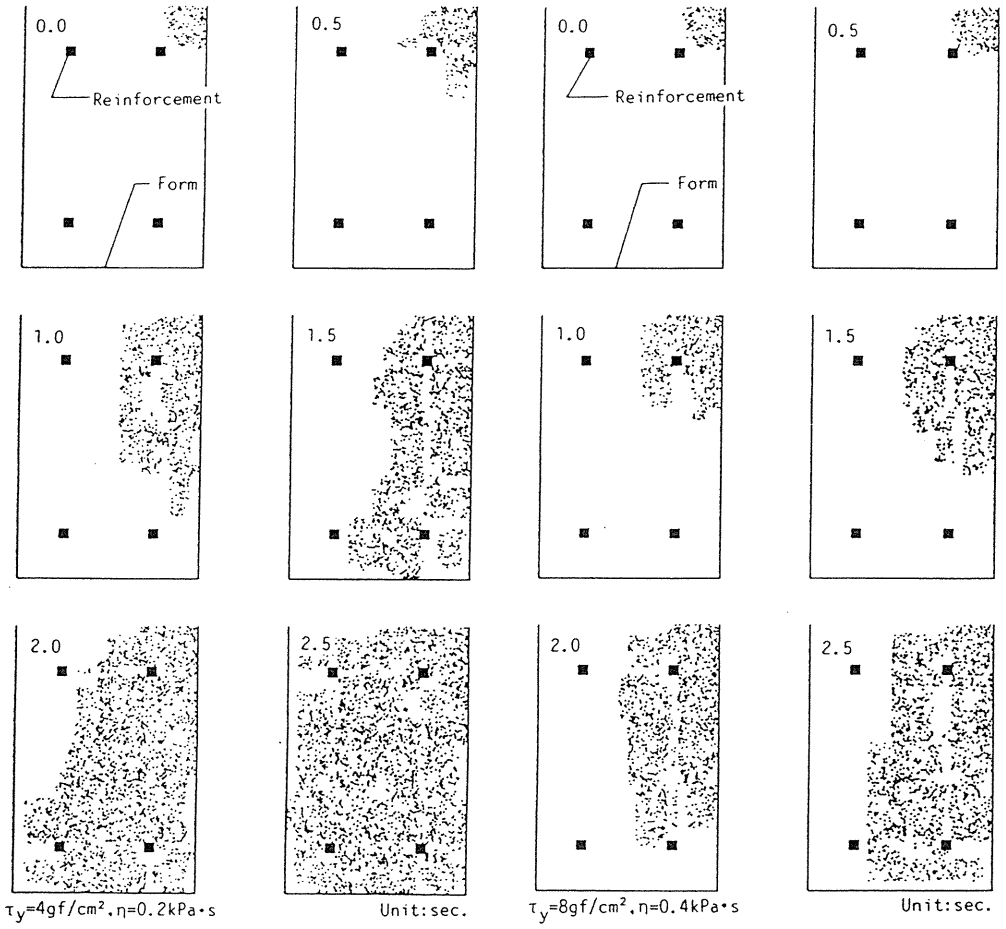

Fig. 82. Analytical result in the case of wet mixed concrete.

Fig. 83. Analytical result in the case of dry mixed concrete.

4. 3 Simulation of Casting into RC Wall

The shape of the RC wall form and the idealization to space divided elements are illustrated in Fig. 84, and some examples of results obtained by the simulation are shown in Fig. 85, where the fresh concrete is cast from three locations. As shown in these figures, this method can be applied to a problem of large deformation such as the behavior of fresh concrete flowing into wide area in the form.

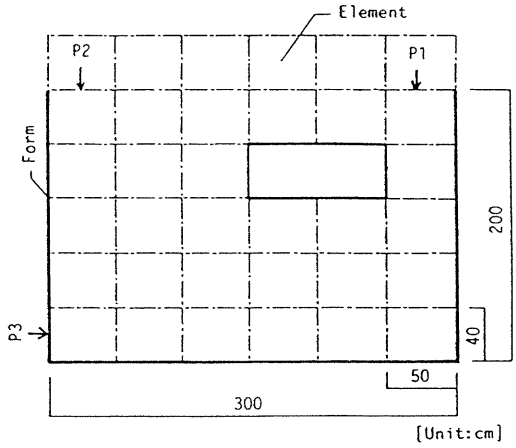

Fig. 84. Form and idealization for simulation.

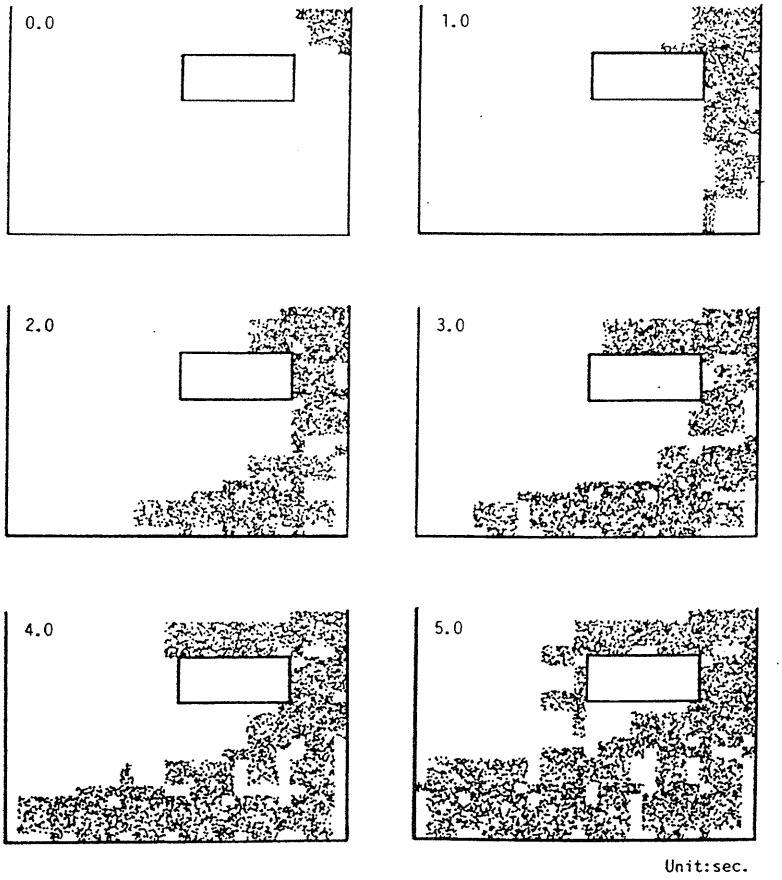

Fig. 85. Example of analytical results. (a) Casting from P1

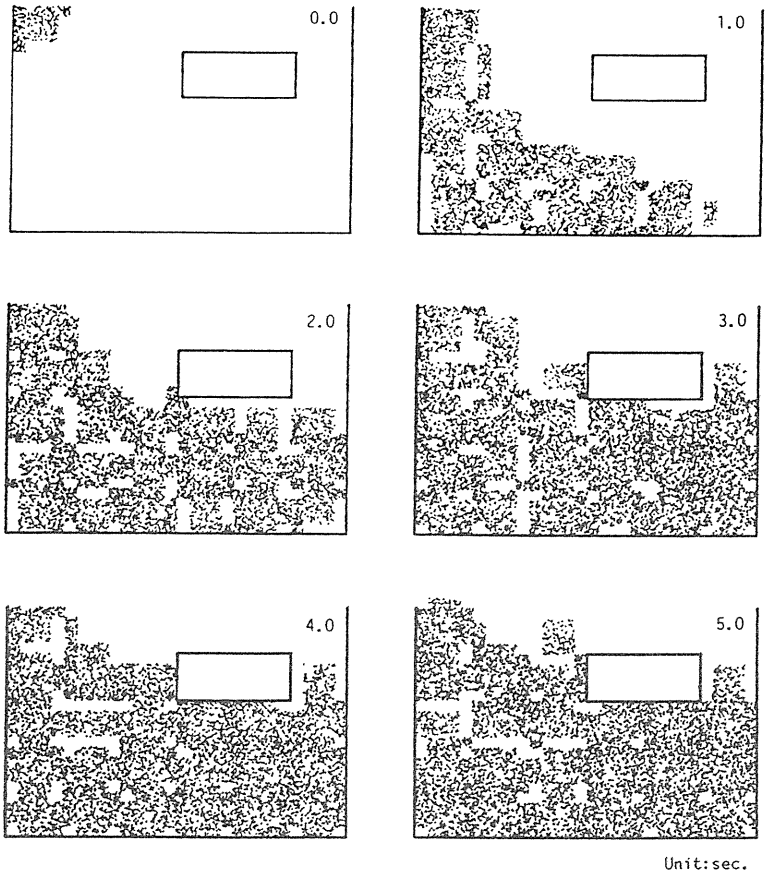

Fig. 85. Example of analytical results. (b) Casting from P2

This analytical method can be also applied to the simulation for considering the effects of vibration, reinforcement, slump loss of concrete with time, etc., by changing the properties of materials in each cell according to the portion or time. An example of analytical model is shown in Fig. 86. The input data of rheological properties are changed at each portion where fresh concrete becomes flowable subjected to vibration, or it is arrested to flow by densely reinforced bars.

The effects of vibration and reinforcement on the flow behavior of concrete are discussed in the following. The shape of form, the idealization to space divided elements and the vibrating points are illustrated in Fig. 87. An example of the simulation for the effect of vibration is shown in Fig. 88.

Fig. 89 shows the arrangement of reinforcement, and Fig. 90 shows the results of simulation. It is apparent by comparing with the results shown in Fig. 85 that the vibration and reinforcement remarkably affect the flow behavior of fresh concrete.

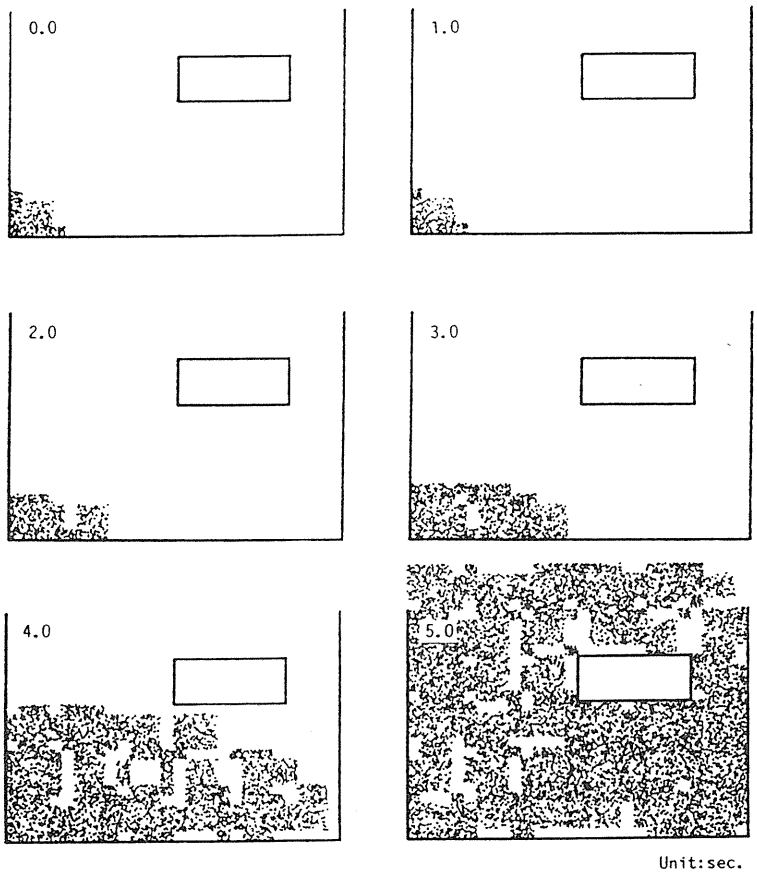

Fig. 85. Example of analytical results. (c) Casting from P3

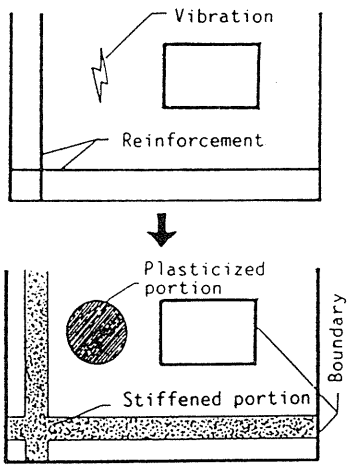

Fig. 86. Idealization of plasticized and stiffened portion.

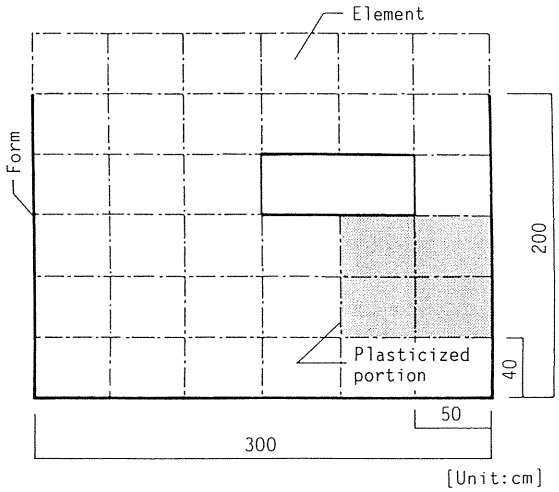

Fig. 87. Form, idealization and plasticized portion.

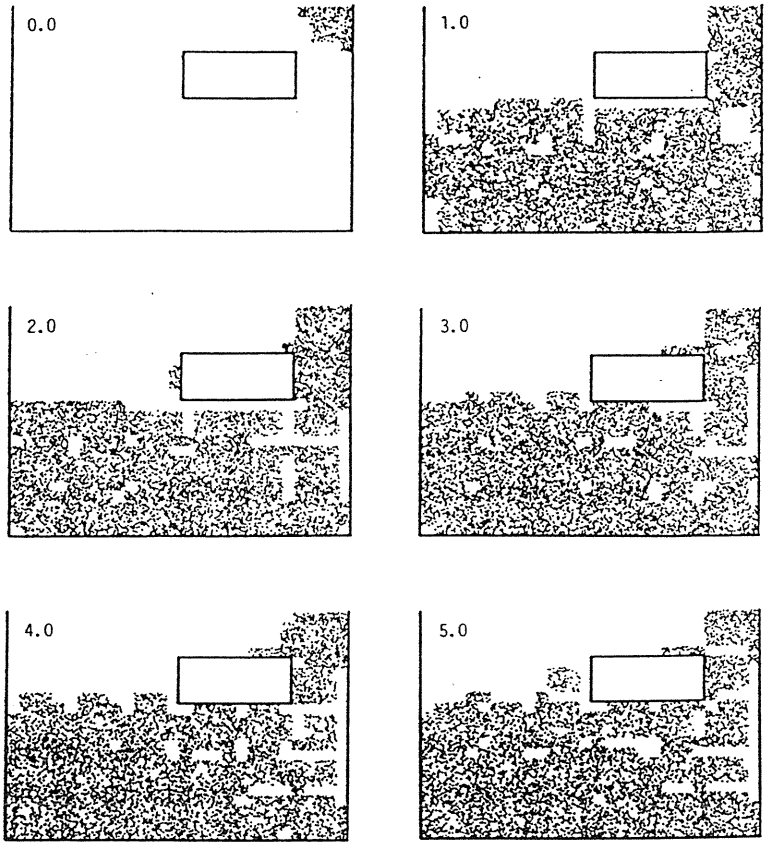

Fig. 88. Example of analytical results.

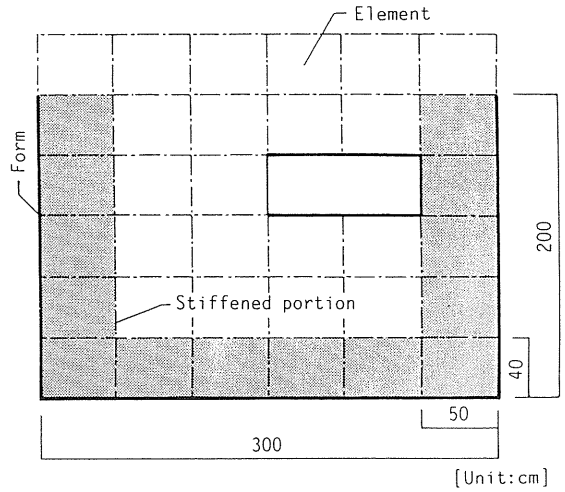

Fig. 89. Form, idealization and stiffened portion.

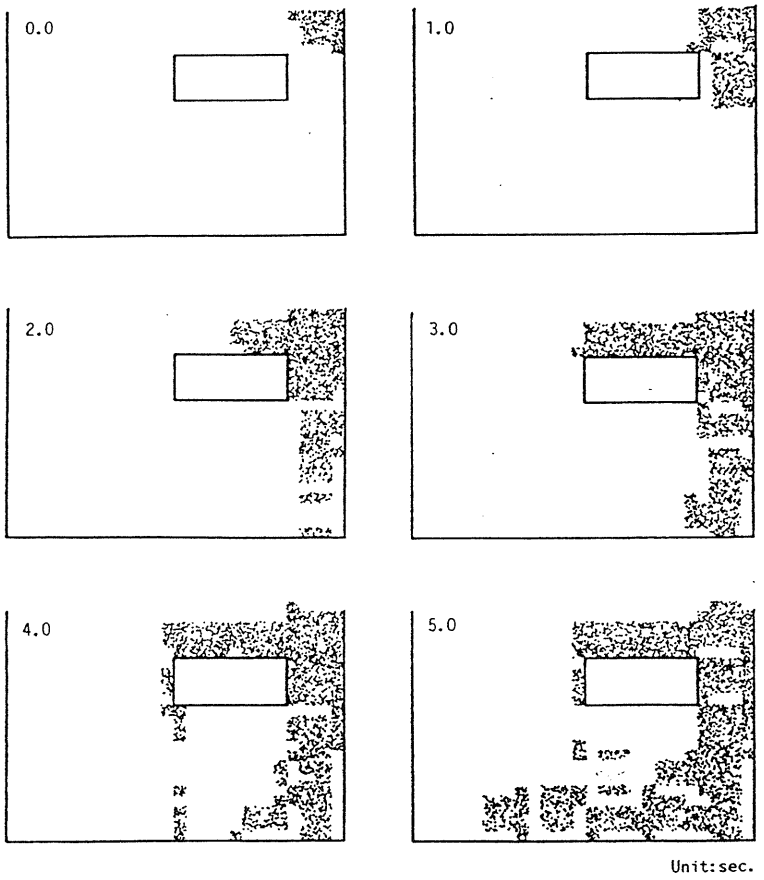

Fig. 90. Example of analytical results.

4. 4 Examination of Analytical Method

The small modeled wall forms analyzed are shown in Fig. 91, which are also prepared for the experiment. The forms with 0, 16 and 25 reinforcing bars (SA, SB and SC form, respectively) were used in this analysis. There was no difference in the flow behavior at the center portion from that at the portion near the surface of wall forms, and the effect of slipping resistance at the surface of wall was not observed in the experiment. Therefore, this analysis was carried out as a two-dimensional problem with no slipping resistance at the surface of wall forms. The casting speed was determined to 0.6 litter per sec. by considering the width of 6 cm for comparing with experimental results. The reinforcing bars were expressed by fixed nodal points in the simulation. The material (concrete) was cast from the left side of 10 cm width as in the same condition as that of the experiment shown in Fig. 92.

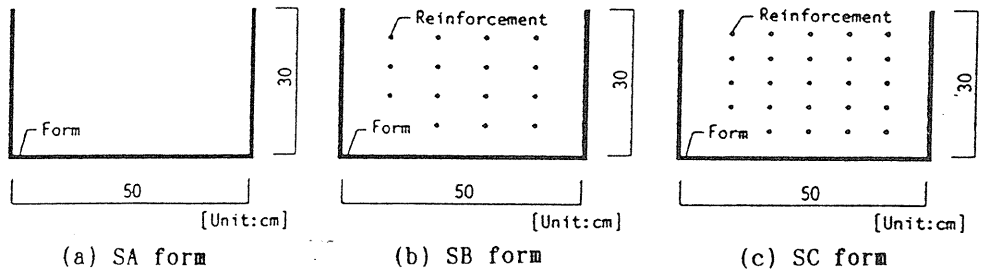

Fig. 91. Modeled wall forms.

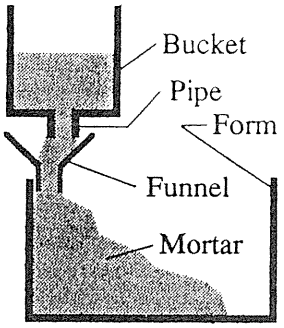

Fig. 92. Apparatus used in the experiment.

There are two approaches to consider the effect of reinforcing bars on the flow behavior of concrete. One is to simulate the flow behavior in wall form without reinforcing bars by using enhanced rheological properties as input data to consider the existence of reinforcing bars, and the other is to simulate directly the flow behavior in wall form with reinforcing bars.

Some results obtained by the analysis and the experiment are shown in Fig. 93, where dots and curves show the analytical and the experimental results, respectively. The flow behavior in SA form is shown in Fig. 93(a). Figs. 93(b) and 93(c) show the analytical results of the flow behaviors in SB and SC forms, respectively, where large rheological constants are

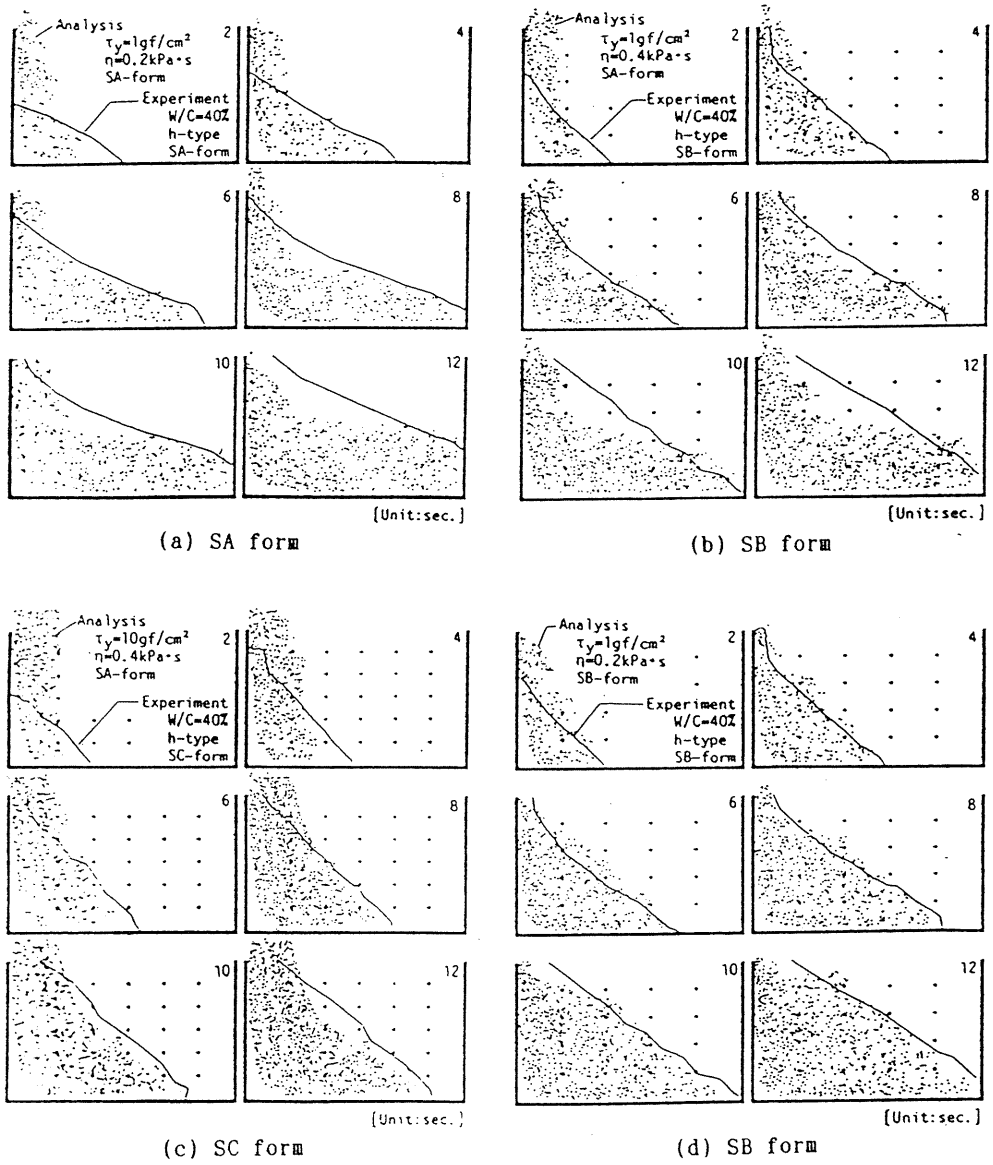

Fig. 93. Comparison between experimental and analytical results.

used and the existence of reinforcing bars are not considered. Fig. 93(d) shows the analytical results of flow behavior in SB form, where all reinforcing bars are directly considered in the analysis.

The analytical flow behaviors are in relatively good agreement with the experimental ones. As shown in Figs. 93(a) to 93(c), the flow speed in the experiment becomes slower with increasing number of reinforcing bars, and rheological constants must be enhanced to about 2 − 10 times larger than real values for simulating these behaviors accurately. The flow

behavior in a different arrangement of reinforcement can be simulated by the analytical method considering the reinforcing bars as boundary condition as shown in Fig. 93(d), and a three-dimensional analysis can be carried out for considering reinforcing bars set in practice. However, it needs a huge calculation time. Therefore, a simple two-dimensional analysis using apparent rheological constants for considering reinforcement is more practical, if enhanced rheological constants can be determined reasonably.

5. Conclusion

In the present paper, three types of analytical methods, viscoplastic finite element method, viscoplastic suspension element method and viscoplastic divided space element method, were proposed for simulating the flow and deformation of fresh concrete. The adequacy of these analytical methods was examined by comparison with some experimental results. Various behaviors of fresh concrete in consistency tests, rheological tests, vibrating tests, pumping in pipe and casting into form and so on, can be estimated analytically by using these simulation methods, and the relationship between the behaviors of fresh concrete in concreting works and the rheological properties can be clarified.

References

1) Popovics, S.: Fundamentals of Portland Cement Concrete, A Quantitative Approach Vol.1: Fresh Concrete, Wiley Interscience Publications, 477pp., 1982.
2) Mizuguchi, H. and Yasunaga, S.: Measurement Method of Yield Value and Plastic Viscosity of Fresh Mortar, Review of the 27th General Meeting, Cement Association of Japan, pp.109–111, 1973.
3) Tattersall, G.H. and Banfill, P.F.G.: The Rheology of Fresh Concrete, Pitman Advanced Publishing Program, 1974.
4) Araki, K., et al.: Relation between Rheological Constants and Mix Factor of Fresh Concrete, Review of the 29th General Meeting, Cement Association of Japan, pp.130–132, 1975.
5) Murata, J.: Flow and Deformation of Fresh Concrete, Matriaux et Constructions, Vol.17, No.98, pp.117–129, 1984.
6) Fung, Y.C.: A First Course in Continuum Mechanics, Prentice-Hall, Inc., 340pp., 1977.
7) Okamoto, H.: Rubbing Resistance between Fresh Concrete and Metal Surface, Proc. of Symposium on Measurement and Analysis of Rheological Properties of Fresh Concrete, Japan Society of Civil Engineers, pp.55–60, 1983 (in Japanese).
8) Murata, J., et al.: Rheology of Fresh Mortar Subjected to Repeated Impact, Proc. of Cement Association of Japan, Vol.37, pp.225–228, 1983 (in Japanese).
9) Wesche, K., et al.: The Influence of Separations on the Rheological Investigation of Cement Paste and Mortar in the Rotation Rheometer, Proc. of RILEM Seminar, Vol.1, pp.2.10-1–2.10-11, 1973.
10) Murata, J. and Kikukawa, H.: Method of Measuring Rheological Constants for Fresh Paste, Mortar and Concrete with Rotation Viscometer, Proc. of the Symposium on Measurement and Analysis of Rheological Properties of Fresh Concrete, Japan Society of Civil Engineers, pp.9–16, 1983 (in Japanese).
11) Murata, J., et al.: Fluidity Analysis of Fresh Concrete by Rotation Viscometer, Review of the 29th General Meeting, Cement Association of Japan, pp.133–135, 1975.
12) Tanigawa, Y., et al.: Constitutive Law and Yield Condition of Fresh Concrete, Trans. of Japan Concrete Institute, Vol.9, pp.47–54, 1987.

13) ACI Committee 309: Behavior of Fresh Concrete during Vibration, Jour. of ACI., Vol.78, No.1–2, pp.36–53, 1981.
14) Tanigawa, Y., et al.: Resistance of Steel Bar Against Flowing of Fresh Concrete Subjected to Vibration, Summaries of Technical Papers of Annual Meeting, Architectural Institute of Japan, A, pp.241–242, 1989 (in Japanese).
15) Nanayakkara, A., et al.: Mathematical Modeling of Deformation of Fresh Concrete in Pumping, Proc. of Japan Concrete Institute, Vol.10, No.2, pp.819–824, 1988.